Journal of Physiology (1993), **462**, *pp.* 197–228
With 14 *figures*
Printed in Great Britain

INTERCONVERSION BETWEEN DISTINCT GATING PATHWAYS OF THE HIGH THRESHOLD CALCIUM CHANNEL IN RAT VENTRICULAR MYOCYTES

BY SYLVAIN RICHARD*†, PIERRE CHARNET† AND JEANNE M. NERBONNE*‡

*From the *Department of Molecular Biology and Pharmacology, Washington University School of Medicine, St Louis, MO, USA and †Centre de Recherches de Biochimie Macromoleculaire, CNRS, INSERM, 34033 Montpellier-Cedex, France*

(*Received 8 April 1992*)

SUMMARY

1. High-voltage-activated Ca^{2+} current (I_{Ca}) waveforms in adult rat ventricular myocytes comprise two components, referred to here as $I_{Ca(fc)}$ and $I_{Ca(sc)}$ to denote the fast and slow components, respectively, of I_{Ca} decay. At all test potentials, the two time constants of I_{Ca} decay, τ_{fc} and τ_{sc}, differ by approximately an order of magnitude. Neither τ_{fc} nor τ_{sc} varies appreciably with test potential, however, suggesting that current inactivation is not markedly voltage dependent.

2. Current activation at all test potentials follows a sigmoidal time course and is best described by a power function with $n = 4$. Deactivation of the currents, examined following variable length depolarizations to various test potentials, however, follows a single exponential time course. In addition, the kinetics of activation and deactivation of $I_{Ca(fc)}$ and $I_{Ca(sc)}$ are indistinguishable.

3. Although both begin to activate at approximately -30 mV, the voltage dependences of $I_{Ca(fc)}$ and $I_{Ca(sc)}$ are distinct: $I_{Ca(fc)}$ peaks at -10 mV and $I_{Ca(sc)}$ peaks at $+10$ mV.

4. The relative amplitudes of $I_{Ca(fc)}$ and $I_{Ca(sc)}$ vary with the holding potential from which the currents are evoked and with the frequency of current activation: hyperpolarized holding potentials and low stimulation frequencies reveal preferential activation of $I_{Ca(fc)}$, whereas depolarized holding potentials and high stimulation frequencies potentiate $I_{Ca(sc)}$. In addition, the observed voltage- and frequency-dependent changes in $I_{Ca(fc)}$ and $I_{Ca(sc)}$ amplitudes are reciprocal.

5. The apparent voltage dependences of steady-state inactivation of $I_{Ca(fc)}$ and $I_{Ca(sc)}$ are also distinct. $I_{Ca(fc)}$ is reduced to approximately 50% of its maximal amplitude at -45 mV, whereas $I_{Ca(sc)}$ is approximately 50% inactivated at -30 mV.

6. Recovery of $I_{Ca(peak)}$ from steady-state inactivation follows a complex time course. Following inactivation at -10 mV, $I_{Ca(peak)}$ recovers at -90 mV to its

‡ To whom correspondence should be addressed at the Department of Molecular Biology and Pharmacology, Box 8103, Washington University School of Medicine, 660 S. Euclid Avenue, St Louis, MO 63110, USA.

MS 1273

maximal value over a biexponential time course; $I_{Ca(peak)}$ then *decreases* over the next several seconds to a steady-state level.

7. The time course of recovery from steady-state inactivation of $I_{Ca(fc)}$ at −90 mV is best described by the sum of two exponentials; the two time constants of recovery differ by approximately a factor of 25. $I_{Ca(sc)}$, in contrast, recovers rapidly and over a single exponential time course to its maximal value. When the recovery time at −90 mV is increased, however, $I_{Ca(sc)}$ amplitude *decreases* slowly and over a single exponential time course to a steady-state level. The time courses of the slow increase in $I_{Ca(fc)}$ and the slow decrease in $I_{Ca(sc)}$ are similar, suggesting that the changes in the two current components are reciprocal.

8. From the experimental data, a model involving two parallel pathways for gating of a single type of high-voltage-activated Ca^{2+} channel was developed which was capable of generating currents with time- and voltage-dependent properties similar to those of I_{Ca} measured in typical adult rat ventricular myocytes.

9. Experimental testing of the predictions of the parallel pathway gating model suggests that the experimentally observed time- and voltage-dependent interconversions between the two gating pathways only occur via the closed states of the channel.

INTRODUCTION

In many cells, depolarization-activated Ca^{2+} current (I_{Ca}) waveforms are complex and appear to reflect the presence and activation of distinct types of voltage-gated Ca^{2+} channels. The suggestion that multiple types of Ca^{2+} channels co-exist, originally made by Hagiwara and co-workers in studies of macroscopic I_{Ca} waveforms in starfish eggs (Hagiwara, Ozawa & Sand, 1975), has been supported by macroscopic and microscopic recordings of Ca^{2+} channel currents in a variety of different cells, including cardiac myocytes (for review, see Bean, 1989; Hess, 1990). These channel types, termed low-voltage-activated (LVA) and high-voltage-activated (HVA) are readily distinguished, based primarily on differing voltage dependences of activation and inactivation, kinetics and pharmacological sensitivities (Bean, 1989; Hess, 1990). LVA and HVA Ca^{2+} channels are co-expressed in atrial and ventricular myocytes from several species (Bean, 1985; Nilius, Hess, Lansman & Tsien, 1985; Mitra & Morad, 1986; Bonvallet & Rougier, 1989; Xu & Best, 1990) and in cells from the rabbit sino-atrial node (Hagiwara, Irisawa & Kameyama, 1988). In several other myocardial preparations, however, only HVA type Ca^{2+} channels appear to be present, i.e. no LVA Ca^{2+} channel currents have been recorded (Argibay, Fischmeister & Hartzell, 1988; Richard, Tiaho, Charnet, Nargeot & Nerbonne, 1990; Ouadid, Seguin, Richard, Chaptal & Nargeot, 1991; LeGrand, Hatem, Deroubaix, Couetil & Coraboeuf, 1991).

Previously we reported that macroscopic HVA Ca^{2+} channel currents in isolated adult rat ventricular myocytes comprise two kinetically distinct components (Richard *et al.* 1990). These components were distinguished based on differing kinetics of inactivation, and were referred to as $I_{Ca(fc)}$ and $I_{Ca(sc)}$ to denote the fast and the slow components, respectively, of I_{Ca} decay. In addition, we demonstrated that $I_{Ca(fc)}$ and $I_{Ca(sc)}$ are differentially regulated by membrane potential and the frequency of channel activation, and are differentially affected by β-adrenergic receptor

stimulation and dihydropyridine Ca^{2+} channel agonists (Richard *et al.* 1990). The presence of two components of decay of macroscopic Ca^{2+} currents could suggest the presence and activation of different types of voltage-gated Ca^{2+} channels (Bean, 1989; Hess, 1990), although other interpretations are certainly also possible. Two components of I_{Ca} decay could, for example, result from two distinct mechanisms of inactivation, such as Ca^{2+}-dependent and voltage-dependent inactivation (Eckert & Chad, 1984), as has been demonstrated in other myocardial preparations (Kass & Sanguinetti, 1984; Lee, Marban & Tsien, 1985). Alternatively, two components of I_{Ca} inactivation could reflect alternate gating pathways of a single population of channels. Biexponential decay of currents through channels encoded by a single mRNA has been observed for voltage-dependent Na^+ (Moorman, Kirsch, Van-Dongen, Joho & Brown, 1990; Zhou, Potts, Trimmer, Agnew & Sigworth, 1991) and K^+ (Koren, Liman, Logothetis, Nadal-Ginard & Hess, 1990) channels expressed in *Xenopus* oocytes. In addition, single channel recordings of rat brain (type III) and μI skeletal Na^+ channels expressed in *Xenopus* oocytes suggest that individual channels can switch between two modes of gating, and that it is this switch that underlies the two components of inactivation of the macroscopic currents (Moorman *et al.* 1990; Zhou *et al.* 1991). It seems possible that a similar mechanism could underlie the behaviour of the HVA Ca^{2+} channels in adult rat ventricular myocytes. Interestingly, it has recently been demonstrated at the single channel level that HVA Ca^{2+} channels in isolated cardiac myocytes display alternate gating modes (Hess, Lansman & Tsien, 1984), and that transitions into the mode with the highest open probability is voltage dependent (Pietrobon & Hess, 1990) and potentiated by β-adrenergic receptor stimulation (Yue, Herzig & Marban, 1990).

In the experiments described here, we have examined the detailed time- and voltage-dependent properties of $I_{Ca(fc)}$ and $I_{Ca(sc)}$ in isolated adult rat ventricular myocytes, and we provide clear evidence that $I_{Ca(fc)}$ and $I_{Ca(sc)}$ reflect alternate pathways for the gating of a single type of HVA Ca^{2+} channel rather than two distinct types of Ca^{2+} channels or the combined presence of Ca^{2+}-dependent and voltage-dependent inactivation mechanisms. In addition, a gating model, developed from the experimental data, is presented. The model is shown to be capable of generating currents with time- and voltage-dependent properties similar to those of Ca^{2+} recorded in typical adult rat ventricular myocytes. Experimental testing of the predictions of this model revealed that interconversions between the two gating pathways probably occur only via the closed states of the channel.

METHODS

Cell isolations. Single ventricular myocytes were isolated from 4–10 week Long Evans rat hearts using a protocol described previously (Apkon & Nerbonne, 1991). Briefly, rats were killed by rapid cervical dislocation, hearts were removed and perfused retrogradely through the aorta (at 37 °C) with 25 ml of Ca^{2+}-free Krebs buffer, followed by 15–30 min with Krebs buffer containing 5–10 μM Ca^{2+} and 0·04–0·2% Type II collagenase (Worthington or Sigma). Following perfusion, the ventricles were chopped, incubated in fresh enzyme solution for 5–10 min and mechanically dispersed. After washing and centrifugation, isolated myocytes were resuspended in serum-free Medium-199 (Irvine) supplemented with antibiotics (penicillin/streptomycin) plated on laminin (Collaborative Research)-coated glass coverslips and maintained at 37 °C in an air–CO_2 (95:5)

environment. Rod-shaped, Ca^{2+}-tolerant myocytes adhere preferentially to laminin, and damaged or rounded-up cells were removed by replacing the culture medium 1 h after plating; thereafter, the medium was exchanged daily.

Although most isolated myocytes remain rod-shaped during the first week *in vitro*, some cells do develop rounded centres, spread along the (laminin) substrate and display spontaneous and rhythmic, contractile activity. If maintained for 2–3 weeks *in vitro*, eventually all cells adopt these 'dedifferentiated' characteristics. The experiments here were performed on rod-shaped ventricular myocytes within the first 3 days after isolation to avoid any complications resulting from dedifferentiation. Neither the waveforms nor the voltage-dependent properties of the currents varied measurably over this time *in vitro*. The electrophysiological properties of 'dedifferentiated' cells were not examined.

Electrophysiological recordings. The whole-cell variation of the patch-clamp technique (Hamill, Marty, Neher, Sakmann & Sigworth, 1981) was employed to record voltage-gated Ca^{2+} channel currents (I_{Ca}) in isolated adult rat ventricular myocytes. All experiments were performed at room temperature (20–22 °C). The voltage-clamp/current-clamp circuit was provided by either a Model 8900 (Dagan, 1 GΩ feedback resistor) or a Biologic (RK 300) whole-cell patch-clamp amplifier. Recording pipettes were fabricated from flint glass and the shanks coated with Sylgard (Dow Corning) to reduce pipette capacitance. Pipettes were fire-polished prior to use to produce electrodes with tip diameters of 1·0–2·0 μm and resistances of 2–4 MΩ when filled with recording solution (see below). After formation of a high resistance 'giga' seal between the recording electrode and the myocyte membrane, electrode capacitance was compensated electronically prior to obtaining a whole-cell recording; seal resistances were in the range of 1–20 GΩ.

In the whole-cell configuration, series resistances (estimated from the decay of the uncompensated capacitative transients) were approximately 1·5–2 times the pipette resistance (Marty & Neher, 1983). Because series resistances were compensated by $\geqslant 80\%$ and current amplitudes were < 5 nA, voltage errors resulting from the uncompensated series resistance were always $\leqslant 8$ mV and were not corrected. Series resistance compensation was checked at regular intervals and data were discarded if increases in series resistance were evident during the course of an experiment. Cell input resistances were in the range of 0·2–2 GΩ and capacitative transients (after compensation) decayed to baseline in all cells in $\leqslant 3$ ms. Voltage-gated inward Ca^{2+} currents (I_{Ca}) were routinely recorded during brief (100–125 ms) depolarizations to test potentials between −40 and +70 mV from holding potentials (V_H) between −90 and −40 mV. Voltage steps were presented in 10 mV increments at 10 s intervals unless otherwise noted. All experimental parameters, such as holding potentials, test potentials, etc., were controlled with an IBM-PC, equipped with a Tecmar Labmaster analog–digital interface (Scientific Solutions) to the electrophysiological equipment, using the pClamp software package (v 4.1, Axon Instruments). Sampling frequencies ranged from 100 Hz to 20 kHz and current signals were filtered at 3–5 kHz prior to digitization and storage.

Solutions. In initial experiments, the bath solution contained (mM): 136 NaCl, 4 KCl, 2 $CaCl_2$, 2 $MgCl_2$, 10 Hepes, and 10 glucose at pH 7·2 (NaOH); 20 μM tetrodotoxin (TTX) was included to suppress voltage-activated Na^+ currents (I_{Na}). Although 20 μM is a relatively high concentration of TTX, complete block of I_{Na} in these cells was not provided (Apkon & Nerbonne, 1991). Because these initial experiments revealed that the TTX-resistant Na^+ current was evident when currents were evoked from holding potentials negative to approximately −60 mV, subsequent experiments were performed using TEACl (136 mM) in place of NaCl in the bath. Control experiments revealed that the substitution of TEA provided complete block of I_{Na} and the total suppression of voltage-activated K^+ currents without measurably affecting the voltage- or time-dependent properties of I_{Ca} (see Results). Recording pipettes routinely contained (mM): 135 CsCl, 10 EGTA, 10 Hepes, 10 glucose, 3 Mg-ATP, and 0·4 Tris-GTP at pH 7·2 (CsOH). In some experiments, the EGTA concentration was lowered to 1·0 mM and, in others, BAPTA (Tsien, 1980) at 10 mM was used in place of EGTA. In addition to maintaining intracellular Ca^{2+} concentrations low, the presence of EGTA (or BAPTA) in the recording pipettes was intended to minimize Ca^{2+}-dependent inactivation of I_{Ca} and to prevent activation of any Ca^{2+}-dependent inward currents (Ehara, Noma & Ono, 1988).

Data analyses. For the most part, the time- and voltage-dependent properties of the currents were analysed using the curve fitting programs in pClamp. Some of the data were compiled and analysed using the spreadsheet, Lotus 1-2-3 (Lotus Corporation). Peak inward Ca^{2+} currents

($I_{Ca(peak)}$) were measured as the difference between the maximal inward current amplitude and the zero current level. Whole cell membrane capacitances were determined from integration of the capacitative currents recorded during 5 mV voltage steps from a V_H of −60 mV. Time constants for current activation during depolarizations from various holding potentials were determined by fitting the expression:

$$I(t) = I_{max}[1-\exp(-t/\tau)]^n,$$

where $I(t)$ is the current at time t, I_{max} is the peak current, τ is the activation time constant and n is a factor that reflects the number of closed states preceding channel opening. Time constants for current deactivation were determined from single exponential fits to the tail currents evoked at various membrane potentials following 10 and 50 ms depolarizations to −10 and +30 mV (see text). For these analyses, capacitative transients were subtracted electronically prior to fitting the data. Current inactivation was best fitted by the sum of two exponential components using the expression:

$$I(t) = I_{Ca(fc)}[\exp(-t/\tau_{fc})]+I_{Ca(sc)}[\exp(-t/\tau_{sc})],$$

where $I_{Ca(fc)}$ and $I_{Ca(sc)}$ are the amplitudes and τ_{fc} and τ_{sc} are the time constants of the fast and slow components of I_{Ca} decay. There was no evidence for a non-inactivating component of I_{Ca} (Richard *et al.* 1990). In all cases, correlation coefficients (r) were calculated to determine the quality of the fits. The zero time was set slightly before the peak of the inward current (I_{Ca}) to determine $I_{Ca(fc)}$ and $I_{Ca(sc)}$ and, in all cases, the sum of $I_{Ca(fc)}$ and $I_{Ca(sc)}$ accounted for the $I_{Ca(peak)}$ current amplitude. In separate analyses, activation and inactivation time constants were obtained from simultaneous fitting of the rising and decay phases of the currents. The time constants obtained from these fits were not significantly different from those obtained from the separate analyses of the rising and the decay phases. All averaged and normalized data are presented as means ± the standard deviation of the mean (±S.D.); statistical significance was examined using the χ^2 test.

Model simulations. For modelling the HVA Ca^{2+} channel currents in adult rat ventricular myocytes, a state diagram was constructed and differential equations were written describing the time-dependent changes in the probability of a channel being in each of the proposed kinetic states as functions of the instantaneous probability of being in connected states and the transition rate constants. Simulations were accomplished using a continuous dynamic system simulation program (TUTSIM, Applied i, Palo Alto, CA, USA) with the instantaneous probabilities over time obtained by numerical integration at a rate of 50 kHz. The modelled currents were generated at the same rate by multiplying the open state probabilities by the driving force, $V_m - V_{rev}$, where V_m is the membrane potential and V_{rev} is the estimated reversal potential for Ca^{2+} of +70 mV. The voltage-dependent activation and deactivation rate constants used in the modelling were those derived from analyses of the observed rates of current activation and deactivation. Similarly, the inactivation and recovery from inactivation rate constants used in the modelling were those derived from the inactivation and recovery data. The various rate constants were adjusted until the model generated currents with time- and voltage-dependent properties similar to those recorded in a typical ventricular cell.

RESULTS

Ca^{2+} current waveforms

Representative voltage-activated inward Ca^{2+} current (I_{Ca}) waveforms evoked in isolated adult rat ventricular myocytes during depolarizing voltage steps from a V_H of −90 mV are displayed in Fig. 1. In general, recordings of I_{Ca} were obtained from small cells (5–10 μm in diameter and 100 μm in length) with whole-cell membrane capacitances (mean ± S.D.) of 142 ± 8 pF (n = 12). In NaCl-containing bath solution, a rapidly activating and inactivating inward current is recorded on depolarizations to potentials ≥ −40 mV (Fig. 1*A*). This current is eliminated when TEACl is substituted for NaCl (Fig. 1*B*), suggesting that it reflects a TTX-resistant component of I_{Na} (Apkon & Nerbonne, 1991). The current–voltage (I–V) relations for I_{Ca} recorded in NaCl- and TEACl-containing bath solutions are indistinguishable (Fig.

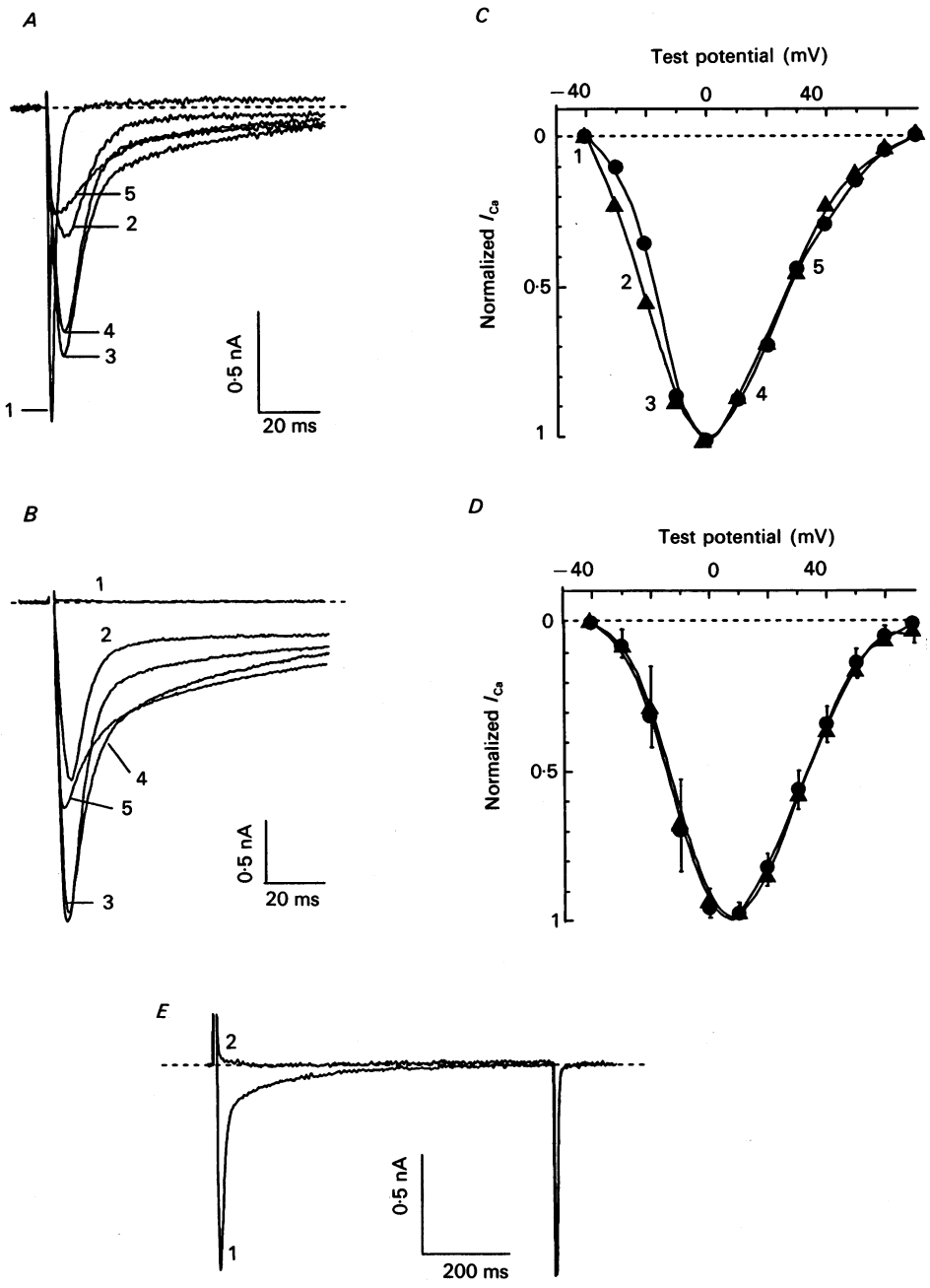

Fig. 1. For legend see facing page

1*C* and *D*). To eliminate contamination from the TTX-resistant component of I_{Na}, therefore, all subsequent experiments were performed in the TEACl-containing bath. In combination with the CsCl in the pipettes, these recording conditions also ensured the blockade of depolarization-activated outward K^+ currents (Apkon & Nerbonne, 1991). Suppression of depolarization-activated K^+ currents was confirmed in some experiments after blockade of I_{Ca} by 2 mM Co^{2+} (Fig. 1*E*). Under these conditions, no inward or outward currents were recorded on depolarizations to potentials between −30 and +70 mV. Thus, we conclude that the current waveforms recorded and analysed here reflect only I_{Ca}, uncontaminated by voltage-activated K^+ currents (see Discussion).

In general, I_{Ca} was recorded within 2–3 min of establishing the whole-cell configuration, and stable recordings were maintained for 5–30 min with no measurable variations in the time- or voltage-dependent properties of the currents and no evidence of 'run-down'. Experiments were terminated if the properties of the currents changed or if 'run-down' became evident. Although I_{Ca} was readily recorded in all cells, there were large variations in absolute current amplitudes: $I_{Ca(peak)}$ amplitudes evoked at +10 mV from a V_H of −90 mV, for example, varied over the range of 500–4400 pA with a mean (±S.D.) of 1720±1000 pA ($n = 17$). These differences were not correlated with cell membrane surface area, suggesting that Ca^{2+} channel densities vary among cells.

Two components of I_{Ca}

On depolarization, I_{Ca} activates rapidly and the time-to-peak I_{Ca} decreases for currents evoked at more positive test potentials (Fig. 1*A* and *B*). Time constants for I_{Ca} activation were determined by fitting the rising phases of the currents using the expression $I(t) = I_{max}[1-\exp(-t/\tau)]^n$ (see Methods). At all test potentials, the current waveforms were best fitted using this expression with $n = 4$. Activation time constants decreased approximately 5-fold over the potential range of −20 to +40 mV (Fig. 2*A*), and are indistinguishable for currents evoked from −90 and −40 mV. These data are well-described by a continuous function of voltage of the

Fig. 1. Waveforms (*A* and *B*) and current–voltage (*I–V*) relations (*C* and *D*) of I_{Ca} in isolated adult rat ventricular myocytes. Currents were recorded during 100 ms depolarizations to test potentials between −40 and +70 mV from a V_H of −90 mV in bath solutions containing 136 mM NaCl (*A*) or 136 mM TEACl (*B*). The bath also contained 2 mM Ca^{2+} as the charge carrier and 10 μM TTX to block I_{Na}. Depolarizing voltage steps were presented in 20 mV increments at 10 s intervals. *A* and *B*, I_{Ca} waveforms recorded at test potentials of −40, −20, −10, +10 and +30 mV are displayed and numbered in order of increasing depolarization, i.e. the currents evoked at −40 mV are labelled '1', those evoked at −20 mV are labelled '2', etc. Note the presence of the rapidly activating and inactivating TTX-resistant component of I_{Na} at −40 mV (trace 1) in the NaCl- (*A*) but not in the TEACl- (*B*) containing bath. *C*, normalized single cell *I–V* relations for $I_{Ca(peak)}$ for the cells in *A* (▲) and *B* (●); the numbers correspond to the current records displayed in *A* and *B*. *D*, mean (±S.D.) normalized *I–V* relations for $I_{Ca(peak)}$ for currents evoked from a V_H of −50 mV and recorded in NaCl- (▲; $n = 21$) or TEACl- (●; $n = 17$) containing bath solutions. *E*, I_{Ca} waveforms evoked during depolarizations to +10 mV from a V_H of −90 mV before (1) and after (2) addition of 2 mM Co^{2+} to the bath. No inward or outward currents were recorded on depolarizations in the presence of Co^{2+} (see text).

form $\tau = 1{\cdot}48[\exp(0{\cdot}020\ V_m)]$ (Fig. 2*A*, continuous line). I_{Ca} decay, in contrast, was best fitted at all test potentials by the sum of two exponential components (Richard *et al.* 1990). The time constants for the fast (τ_{fc}) and the slow (τ_{sc}) components of I_{Ca} decay differ by approximately an order of magnitude and are indistinguishable for

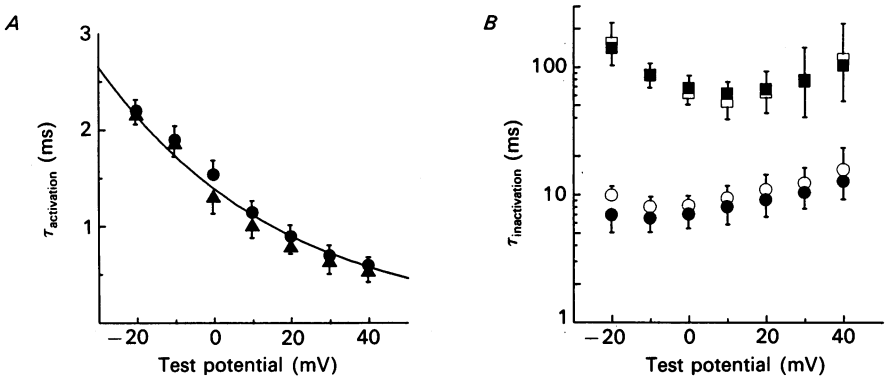

Fig. 2. Kinetics of I_{Ca} activation (*A*) and inactivation (*B*). Currents were recorded as described in the legend of Fig. 1 in TEACl-containing bath solution. *A*, to determine the time constants for I_{Ca} activation ($\tau_{activation}$) for the currents evoked during membrane depolarizations to test potentials between −20 and +40 mV from holding potentials of −90 (●) and −40 (▲) mV, the rising phases of the currents were fitted using the expression $I(t) = I_{max}[1-\exp(-t/\tau)]^4$ (see Methods). Mean (±S.D.; $n = 5$) values are plotted as a function of test potential. The continuous line is the best fit to the data points. *B*, time constants for I_{Ca} inactivation ($\tau_{inactivation}$) were determined from double exponential fits to the decay phases of the currents as described in Methods. Mean (±S.D.; $n = 17$) values for τ_{fc} (●, ○) and τ_{sc} (■, □) are plotted as a function of test potential for currents evoked from holding potentials of −90 (●, ■) and −40 (○, □) mV.

currents evoked from −90 and −40 mV (Fig. 2*B*). Both time constants vary only slightly with test potential: (mean±S.D.; $n = 17$) τ_{fc} values, for example, were 6·6±2·1 ms at −10 mV and 13·0±3·9 ms at +40 mV; and (mean+S.D.; $n = 17$) τ_{sc} values were 63±23 ms at −10 mV and 104±48 ms at +40 mV. Over the entire range of voltages examined, therefore, τ_{fc} and τ_{sc} vary by less than twofold. In contrast to what would be expected for a voltage-dependent component of I_{Ca} inactivation (Fox, 1981; Kass & Sanguinetti, 1984), the trend for both time constants is to *increase* with increasing depolarization (Fig. 2*A*), rather than to *decrease*. These findings suggest that neither component of I_{Ca} inactivation is markedly voltage dependent. In addition, neither τ_{fc} nor τ_{sc} varies appreciably as a function of I_{Ca} amplitude (Figs 2*B* and 3), suggesting that inactivation also does not appear to be Ca^{2+} dependent (Eckert & Chad, 1984). Nevertheless, both time constants for I_{Ca} decay are approximately 10 times faster than those seen when either Ba^{2+} or Sr^{2+} is used in place of Ca^{2+} as the charge carrier (data not shown, but see Richard *et al.* 1990). The simplest interpretation of these results is that the rates of inactivation of both current components are Ca^{2+} sensitive, even though they might not be considered Ca^{2+} dependent according to established criteria (Eckert & Chad, 1984) (see Discussion).

Double exponential fits to the decay phases of the currents also revealed that the voltage dependences of $I_{Ca(fc)}$ and $I_{Ca(sc)}$ are distinct. Although both components begin to activate at approximately −30 mV, $I_{Ca(fc)}$ peaks at −10 mV and $I_{Ca(sc)}$ peaks at +10 mV (Fig. 3*A*). In addition, the fast component of I_{Ca} decay, $I_{Ca(fc)}$, is

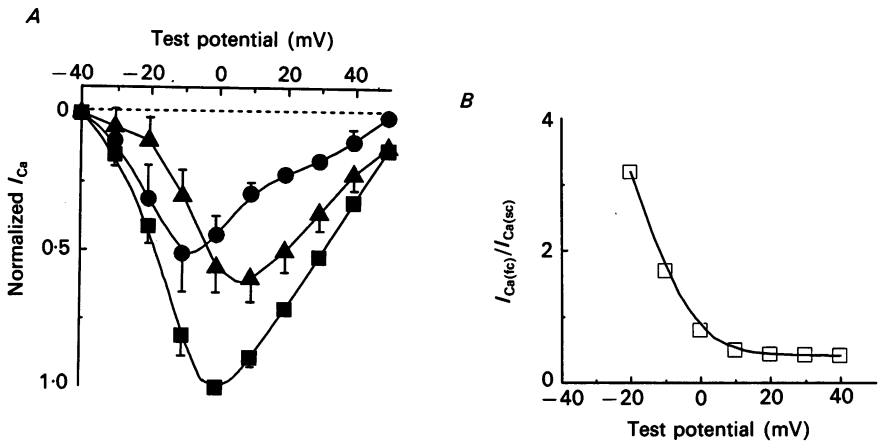

Fig. 3. The *I–V* relations for $I_{Ca(fc)}$ and $I_{Ca(sc)}$ are distinct. *A*, normalized *I–V* relations for $I_{Ca(peak)}$ (■), $I_{Ca(fc)}$ (●) and $I_{Ca(sc)}$ (▲). Currents were recorded in TEACl-containing bath solution as described in the legend of Fig. 1 during depolarizations to potentials between −40 and +50 mV from a V_H of −90 mV. The amplitude of $I_{Ca(peak)}$ in each cell was measured at each test potential and normalized to the peak current amplitude evoked on depolarization to 0 mV in the same cell. $I_{Ca(fc)}$ and $I_{Ca(sc)}$ amplitudes were determined at each test potential from double exponential fits to the decay phases of the currents as described in Methods, and were also normalized to $I_{Ca(peak)}$ amplitude at 0 mV in the same cell. Mean normalized values for $I_{Ca(peak)}$ (■), $I_{Ca(fc)}$ (●) and $I_{Ca(sc)}$ (▲) were then determined and are plotted here ±S.D. ($n = 17$). *B*, the ratio of the amplitudes of $I_{Ca(fc)}$ and $I_{Ca(sc)}$ varies as a function of the test potential. The values plotted are averages and were calculated from the mean normalized *I–V* data in *A*.

the dominant component at hyperpolarized test potentials, whereas the slow component of I_{Ca} decay, $I_{Ca(sc)}$, is the dominant component at potentials positive to approximately 0 mV. In Fig. 3*B*, the ratio $I_{Ca(fc)}/I_{Ca(sc)}$ is plotted as a function of test potential. As is evident, this ratio decreases with increasing depolarization over the voltage range of −20 to +10 mV, but is nearly constant at more positive potentials. These findings suggest that subtle differences in I_{Ca} decay kinetics and in the peak *I–V* relations for I_{Ca} measured in adult rat ventricular myocytes result from variations in the relative amplitudes of $I_{Ca(fc)}$ and $I_{Ca(sc)}$. When $I_{Ca(fc)}$ is larger than $I_{Ca(sc)}$, for example, $I_{Ca(peak)}$ will be recorded near −10 mV, whereas when $I_{Ca(sc)}$ is larger, $I_{Ca(peak)}$ will be recorded closer to +10 mV.

The kinetics of I_{Ca} deactivation were determined from analyses of current tails recorded on membrane hyperpolarizations to various potentials presented approximately 20 ms after the onset of depolarizations to −10 (Fig. 4*A*) or +30 (Fig. 4*B*) mV to evoke I_{Ca}. These depolarizing test potentials were selected because of the differences in the peak *I–V* relations for $I_{Ca(fc)}$ and $I_{Ca(sc)}$ (Fig. 3*A*): tail currents recorded following depolarizations to −10 mV (Fig. 4*A*) should reflect predominately deactivation of $I_{Ca(fc)}$, whereas tail currents recorded following depolarizations to

+30 mV (Fig. 4*B*) should reflect primarily the deactivation of $I_{Ca(sc)}$. At all potentials, the current tails were well fitted by single exponentials with time constants that decreased at the more hyperpolarized potentials (Fig. 4*C*). In addition, the deactivation time constants determined from analyses of the tail

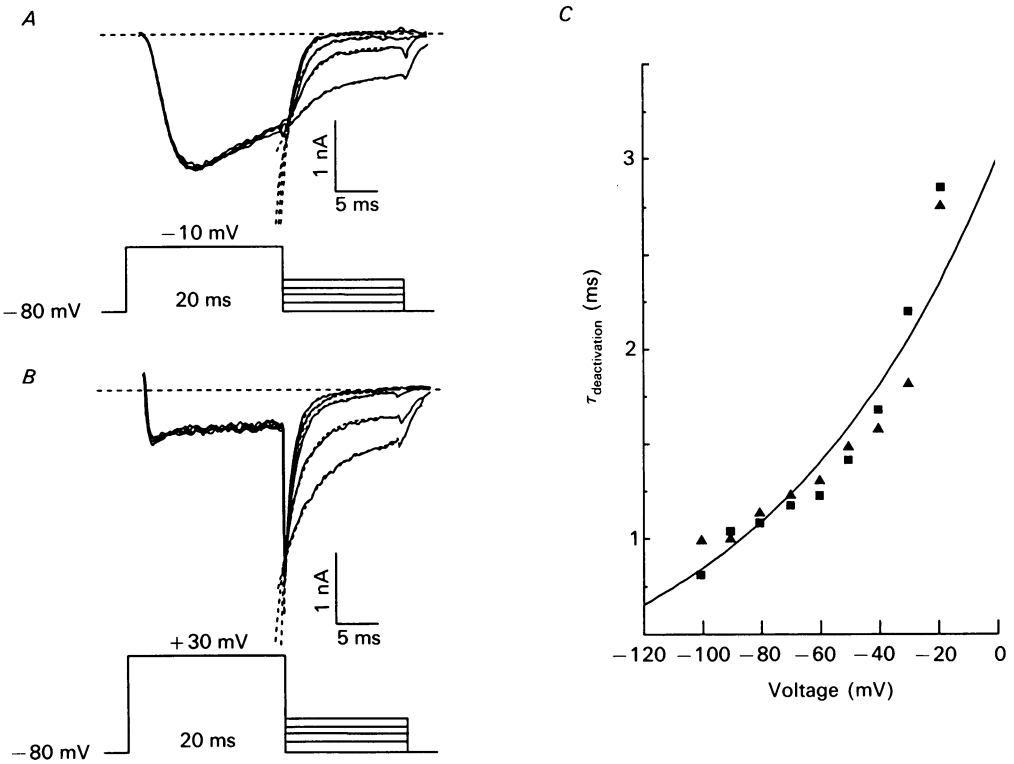

Fig. 4. I_{Ca} deactivation follows a single exponential time course. Currents were recorded as described in the legend of Fig. 1 in TEACl-containing bath solution. *A*, tail currents recorded on membrane hyperpolarizations to potentials between −20 and −80 mV delivered 20 ms after the onset of test depolarizations to −10 mV (from a V_H of −80 mV) to evoke I_{Ca}. *B*, tail currents recorded in the same cell as in *A* on membrane hyperpolarizations to potentials between −20 and −80 mV presented 20 ms after the onset of test depolarizations to +30 mV (from a V_H of −80 mV) to evoke I_{Ca}. In both *A* and *B*, single exponential fits to the tail current decays are plotted (dashed lines) superimposed on the data (continuous lines). The time constants obtained from the fits to the records in *A* were 4·5, 2·7, 2·1, 1·6 and 1·4 ms for hyperpolarizations to −20, −30, −40, −60 and −80 mV. The values for the records in *B* were 4·7, 2·7, 1·9, 1·4 and 1·3 ms at −20, −30, −40, −60 and −80 mV. *C*, mean ($n = 5$) deactivation time constants ($\tau_{deactivation}$) for the tail currents recorded on hyperpolarizations to various potentials 20 ms after the onset of test depolarizations to −10 (▲) and +30 (■) mV in experiments such as those illustrated in *A* and *B*. The continuous line is the best fit to the data points (see text).

currents recorded following depolarizations to −10 and +30 mV are indistinguishable (Fig. 4*C*). These data are well described by a continuous function of voltage of the form $\tau = 3{\cdot}1[\exp(0{\cdot}013\ V_m)]$ (Fig. 4*C*, continuous line).

Voltage- and frequency-dependent changes in I_{Ca} waveforms

Interestingly, I_{Ca} waveforms in adult rat ventricular myocytes vary as a function of the holding potential from which the currents are evoked (Richard *et al.* 1990). As illustrated in Fig. 5, I_{Ca} waveforms recorded (in the same cell) during depolarizations

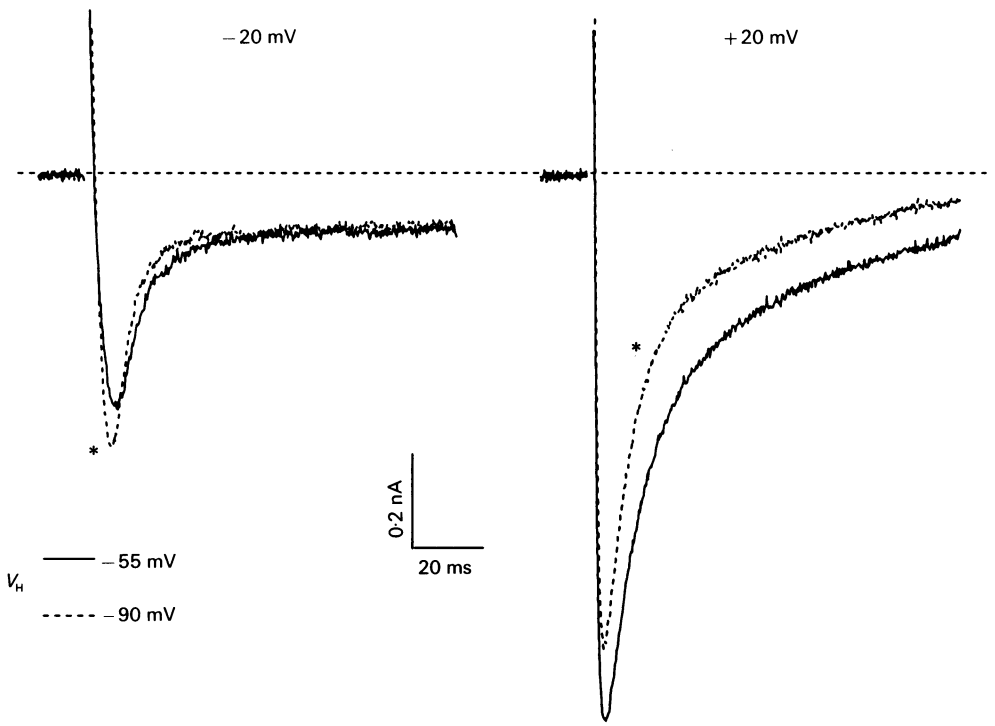

Fig. 5. I_{Ca} waveforms vary with the holding potential from which the currents are evoked. I_{Ca} waveforms, evoked from holding potentials of −90 (dashed lines; *) and −55 (continuous lines) mV, were recorded as described in the legend of Fig. 1 in TEACl-containing bath solution; all records were obtained from the same cell. On depolarizations to −20 mV (left), $I_{Ca(peak)}$ amplitude is larger for the current evoked from a V_H of −90 mV (*). On depolarizations to +20 mV (right), in contrast, $I_{Ca(peak)}$ amplitude is larger for the current evoked from a V_H of −55 mV. Interestingly, at both test potentials, the peak I_{Ca} occurs slightly earlier and the rate of decay of the current appears faster for the currents evoked from −90 mV compared to those evoked from −55 mV. Analyses of the kinetics of current activation and inactivation, however, reveal no differences in the time constants of activation or inactivation as a function of V_H (see text and Fig. 2).

to different potentials from holding potentials of −90 and −55 mV are distinct. On depolarizations to −20 mV, for example, the currents evoked from −90 mV are larger than those evoked from −55 mV. At +20 mV, however, I_{Ca} amplitudes evoked from −55 mV are larger than those evoked from −90 mV (Fig. 5). Macroscopic current kinetics also appear to vary with holding potential in that the time-to-peak I_{Ca} is less and the currents decay more rapidly at all test potentials when the currents are evoked from −90 mV than from −55 mV. Because the time

constants of I_{Ca} activation (Fig. 2*A*) and inactivation (Fig. 2*B*) do not vary measurably as a function of the holding potential from which the currents are evoked, however, the variations in macroscopic current kinetics are most simply interpreted as reflecting differences in the relative contributions of $I_{Ca(fc)}$ and $I_{Ca(sc)}$ to the measured current waveforms at different holding potentials (see below).

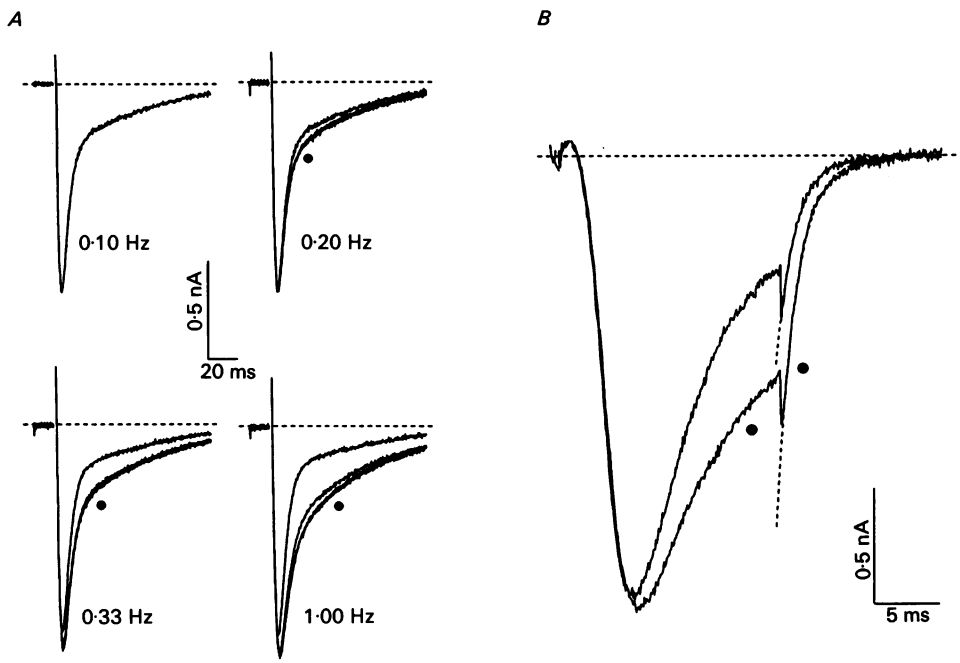

Fig. 6. Increasing the frequency of current activation potentiates $I_{Ca(peak)}$ and slows I_{Ca} decay. *A*, currents, evoked during repetitive depolarizations to +10 mV from a V_H of −90 mV, were recorded as described in the legend of Fig. 1 in TEACl-containing bath solution; four successive depolarizations are displayed in each panel, and the fourth in each panel is indicated by the dot. At 0·1 Hz, I_{Ca} waveforms are stable. At 0·2 Hz, I_{Ca} decay is slowed in the second depolarization, although there are no further changes in I_{Ca} waveforms evident in the subsequent depolarizations. When the frequency is increased further to 0·33 Hz, there is a more marked slowing of I_{Ca} decay and $I_{Ca(peak)}$ amplitude also increases. Again, the change in I_{Ca} is stable on the second depolarization. At 1·0 Hz, there is a further increase in $I_{Ca(peak)}$ amplitude and a slowing of I_{Ca} decay, although in this case the changes in the current waveform do not reach steady state until the third depolarization. *B*, I_{Ca} waveforms recorded as in *A* at 1·0 Hz, and displayed on a faster time scale. The unmarked trace was recorded first and the trace with the dot was recorded 1 s later. Note that, in spite of the slight increase in $I_{Ca(peak)}$ amplitude and the marked slowing of I_{Ca} decay, the kinetics of I_{Ca} activation and deactivation are indistinguishable (see text). The deactivation time constants for the two records illustrated, for example, were 1·72 and 1·75 ms.

I_{Ca} waveforms in these cells also vary as a function of the frequency of current activation (Richard *et al.* 1990). As illustrated in Fig. 6*A*, for example, when the interval between successive depolarizations is reduced from 10 to 5 s, I_{Ca} decay is slowed. When the interpulse interval is further decreased to 3 or 1 s, there is a more

marked slowing of I_{Ca} decay and $I_{Ca(peak)}$ amplitude is increased. Similar results were obtained in many cells and, on average, the amplitudes of $I_{Ca(peak)}$ for the currents evoked at +10 mV from a V_H of −90 mV were increased 7±4% ($n = 13$) when the frequency of current activation was increased from 0·1 to 1 Hz. In contrast to the marked slowing of I_{Ca} decay, however, the kinetics of I_{Ca} activation and deactivation were unaffected by the stimulation frequency (Fig. 6*B*). Double exponential fits to the decay phases of the currents revealed that increasing the rate of stimulation results in a reduction in the amplitude of $I_{Ca(fc)}$ and a corresponding increase in the amplitude of $I_{Ca(sc)}$; there were no measurable changes in τ_{fc} or τ_{sc} when the frequency of current activation was increased. Similar to the changes in I_{Ca} waveforms observed when holding potential is changed (Fig. 5), therefore, the increase in $I_{Ca(peak)}$ amplitude, the increase in the time-to-peak I_{Ca}, and the slowing of I_{Ca} decay are most simply interpreted as reflecting the increase in $I_{Ca(sc)}$ and the corresponding decrease in $I_{Ca(fc)}$.

In contrast to the results presented above, no measurable voltage- or frequency-dependent effects were seen when either Ba^{2+} or Sr^{2+} was used ($n = 20$) as the charge carrier through voltage-activated Ca^{2+} channels in isolated adult rat ventricular myocytes (data not shown). These results may reflect differences in the kinetic properties of the Ba^{2+} and Sr^{2+} currents (Richard *et al.* 1990), as compared to the Ca^{2+} currents (see Discussion).

Steady-state inactivation of $I_{Ca(peak)}$, $I_{Ca(fc)}$ and $I_{Ca(sc)}$

To examine the voltage dependence of steady-state inactivation of I_{Ca}, cells were voltage clamped at −90 mV and subsequently depolarized to conditioning potentials between −80 and −20 mV for 5 s prior to voltage steps to +10 mV to evoke I_{Ca}. The 5 s conditioning pulse duration was selected because no further changes in I_{Ca} waveforms were evident during conditioning pulses lasting up to 30 s (see below). However, substantial, and irreversible, 'run-down' of I_{Ca} was evident during prolonged depolarizations (i.e. lasting minutes) even at potentials negative to threshold for current activation. When cells were voltage clamped at −45 mV for 5 min, for example, $I_{Ca(peak)}$ amplitudes at +10 mV decreased by 40±12% ($n = 12$), and no recovery was observed even after prolonged hyperpolarizations to −90 mV (data not shown). Similar results have been reported previously by others (Schouten & Morad, 1989), and we have not investigated this phenomenon in greater detail. In the experiments here, the effects of changing the membrane potential on I_{Ca} waveforms were examined using the conditioning pulse protocol illustrated in Fig. 7*A*. Normalized $I_{Ca(peak)}$ amplitudes at +10 mV as a function of the conditioning voltage are plotted in Fig. 7*B*. Peak I_{Ca} was 50% inactivated at approximately −35 mV, suggesting that closed I_{Ca} channels can inactivate without opening.

Double exponential fits to the decay phases of the currents evoked at +10 mV from each conditioning potential provided the amplitudes of $I_{Ca(fc)}$ and $I_{Ca(sc)}$ in each cell. Mean (±S.D.; $n = 13$) normalized steady-state inactivation curves for $I_{Ca(fc)}$ and $I_{Ca(sc)}$ are plotted in Fig. 7*B*. These analyses also confirmed that τ_{fc} and τ_{sc} are not measurably altered as a function of holding potential (Fig. 7*C*). The changes in I_{Ca} waveforms observed for currents evoked from various conditioning potentials (Fig. 7*A*), therefore, appear to reflect only modifications in the relative amplitudes

of $I_{Ca(sc)}$ and $I_{Ca(fc)}$. In addition, the finding that $I_{Ca(sc)}$ amplitudes increased when the conditioning potential was decreased from −90 to −50 mV while $I_{Ca(fc)}$ amplitudes decreased suggests that the increase in $I_{Ca(sc)}$ and the decrease in $I_{Ca(fc)}$ could be related. There was no potentiation of the peak inward current as a function of the

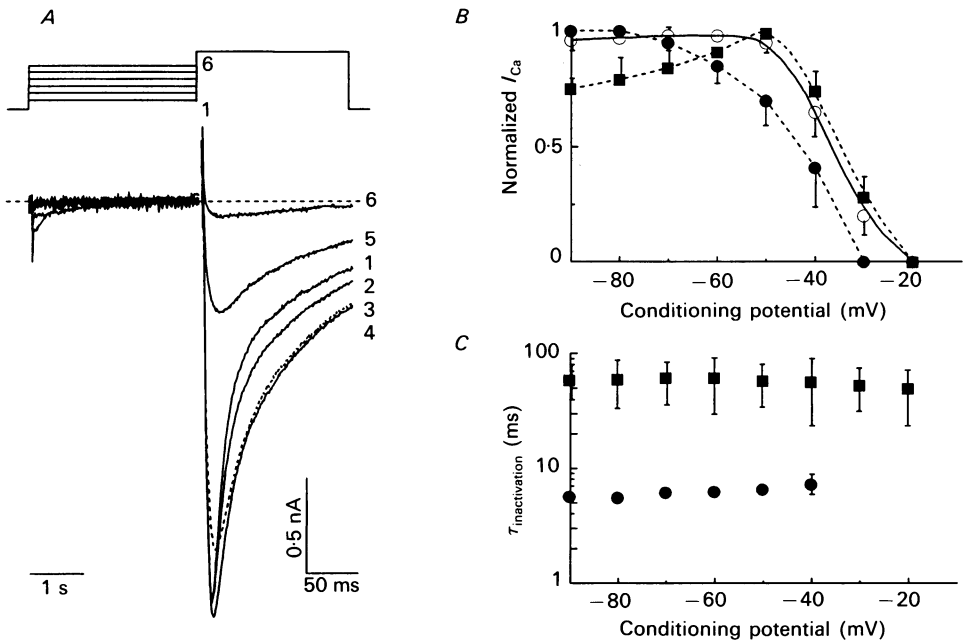

Fig. 7. $I_{Ca(fc)}$ and $I_{Ca(sc)}$ display different sensitivities to voltage-dependent steady-state inactivation. Currents, evoked at +10 mV following 5 s conditioning pulses to potentials between −90 and −20 mV, were recorded in TEACl-containing bath solution as described in the legend of Fig. 1. *A*, representative current waveforms evoked at +10 mV following 5 s conditioning pulses to test potentials between −70 (1) and −20 (6) mV in 10 mV increments; the protocol is illustrated above the current records with the corresponding record numbers included. *B*, mean normalized steady-state inactivation curves for $I_{Ca(peak)}$, $I_{Ca(fc)}$ and $I_{Ca(sc)}$. In each cell, $I_{Ca(peak)}$ amplitudes evoked at +10 mV from each conditioning potential were measured and normalized to the peak current evoked directly from −90 mV. $I_{Ca(fc)}$ and $I_{Ca(sc)}$ were determined from double exponential fits to the decay phases of the currents evoked from each conditioning potential and were normalized to their respective amplitudes evoked directly from −90 mV in the same cell. Mean (±S.D.; $n = 13$) normalized values for $I_{Ca(peak)}$ (○), $I_{Ca(fc)}$ (●), and $I_{Ca(sc)}$ (■) were then calculated and are plotted as a function of conditioning potential. *C*, in contrast to the current amplitudes, mean (±S.D.; $n = 13$) values for τ_{fc} (●) and τ_{sc} (■) do not vary measurably as a function of the conditioning potential from which the currents are evoked. Thus, the variations in I_{Ca} waveforms with conditioning potential (*A*) result only from changes in relative amplitudes of $I_{Ca(fc)}$ and $I_{Ca(sc)}$ (see text).

conditioning potential when either Ba^{2+} or Sr^{2+} was used ($n = 20$) as the charge carrier through voltage-activated Ca^{2+} channels. Again, this difference may reflect the distinct kinetic properties of the currents with Ca^{2+} as the charge carrier (see Discussion).

Recovery from steady-state inactivation

The time dependence of I_{Ca} recovery from inactivation was studied using the voltage-clamp protocol illustrated in Fig. 8*A*. Following a 5 s conditioning pulse at −10 mV to inactivate I_{Ca} completely (Fig. 7), the cell in Fig. 8 was hyperpolarized

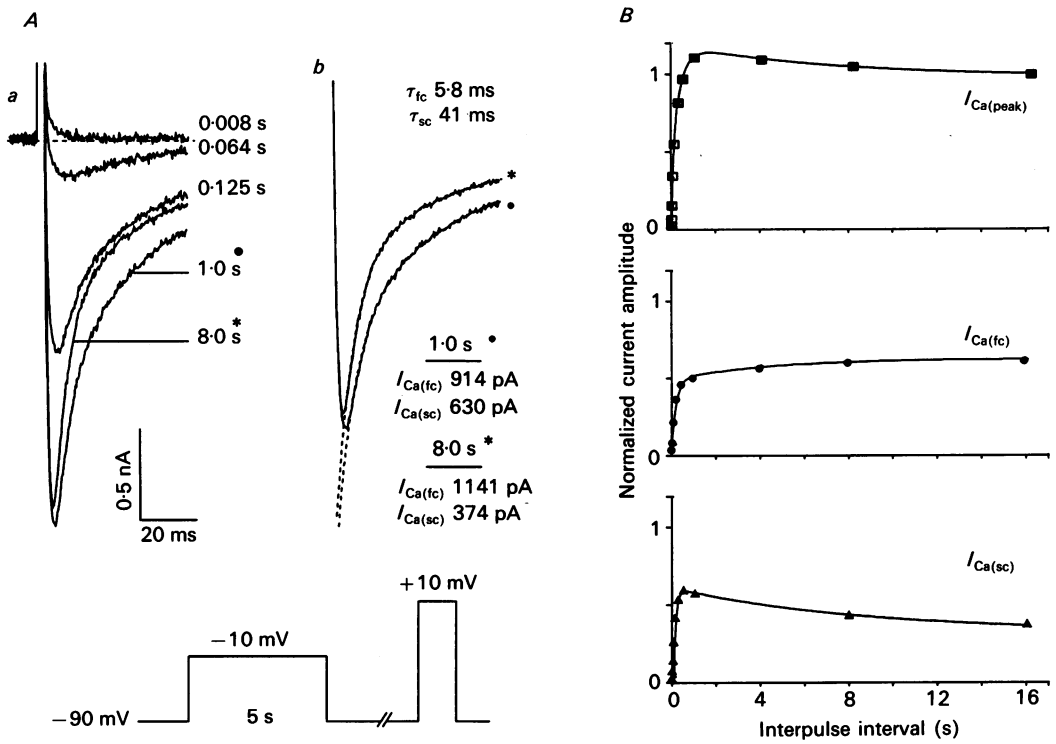

Fig. 8. Recovery of I_{Ca} from steady-state inactivation. *A a*, to examine the time course of recovery from steady-state inactivation, cells were first depolarized to −10 mV for 5 s, followed by a variable length hyperpolarization to −90 mV. I_{Ca} waveforms, evoked during membrane depolarizations to +10 mV, were then recorded; the voltage-clamp protocol is illustrated below the current records. The waveforms displayed are those recorded at +10 mV when the interpulse intervals were 8 ms, 64 ms, 125 ms, 1 s and 8 s. Note that when the recovery period at −90 mV was increased from 1 to 8 s, $I_{Ca(peak)}$ amplitude decreased slightly and current decay was accelerated. *Ab*, double exponential fits (dashed lines) to the decay phases of the currents recorded following interpulse intervals of 1 and 8 s. $I_{Ca(fc)}$ amplitude increases and $I_{Ca(sc)}$ amplitude decreases when the interpulse interval is increased from 1 to 8 s; neither τ_{fc} nor τ_{sc} is altered when the interpulse interval is varied. *B*, time course of recovery from steady-state inactivation for $I_{Ca(peak)}$, $I_{Ca(fc)}$ and $I_{Ca(sc)}$ for the cell in *A*. $I_{Ca(peak)}$ amplitude at each interpulse interval was measured and normalized to the steady-state $I_{Ca(peak)}$ amplitude. The amplitudes of $I_{Ca(fc)}$ and $I_{Ca(sc)}$ were obtained from double exponential fits to the decay phases of the currents recorded at the various interpulse intervals. The amplitudes of each component were normalized to the steady-state $I_{Ca(peak)}$ amplitude, and are plotted here as a function of the interpulse interval.

to −90 mV for varying times prior to the test depolarizations to +10 mV to evoke I_{Ca}. $I_{Ca(peak)}$ amplitude recovers rapidly at −90 mV to a maximal value, recorded when the interpulse interval was 1 s (Fig. 8*A a*). In addition, the recovery of $I_{Ca(peak)}$ to its maximal value follows a double exponential time course with time constants (in this cell) of 76 and 353 ms (Fig. 8*B*). Interestingly, however, when the recovery period at −90 mV was increased further (Fig. 8*A a*), $I_{Ca(peak)}$ amplitude *decreased*, indicating that steady state had not been reached at 1 s. Associated with the decrease in $I_{Ca(peak)}$ amplitude, the apparent rate of current decay was markedly accelerated (Fig. 8*A a*). Double exponential fits to the decay phases of the currents (Fig. 8*A b*) revealed that the changes in the current waveforms reflect an increase in $I_{Ca(fc)}$ and a corresponding decrease in $I_{Ca(sc)}$; neither τ_{fc} nor τ_{sc} was affected. There were no further changes in $I_{Ca(peak)}$ amplitudes or kinetics when longer recovery periods (up to 64 s) were used (data not shown). For the cell in Fig. 8, the slow decrease in $I_{Ca(peak)}$ amplitude to its final steady-state value was best described by a single exponential with a time constant of 7092 ms. Similar results were obtained in experiments conducted on twelve cells, and mean (±S.D.; $n = 12$) normalized recovery data for $I_{Ca(peak)}$ at −90 mV are plotted in Fig. 9*B*. In all cells examined, the maximal peak I_{Ca} was recorded when the recovery period at −90 mV was approximately 1 s. In addition, the mean normalized data for recovery of $I_{Ca(peak)}$ to its steady-state level at −90 mV (Fig. 9*B*) are well described by the sum of three exponentials with time constants (±S.D.) of 77±6, 875±543 and 5053±2596 ms.

Double exponential fits to the decay phases of the currents recorded at +10 mV following variable length repolarizations to −90 mV revealed that the time courses of recovery of $I_{Ca(fc)}$ and $I_{Ca(sc)}$ are also distinct (Fig. 8). There are, for example, two distinct phases of $I_{Ca(fc)}$ recovery: the initial recovery phase is rapid, although $I_{Ca(fc)}$ amplitude continues to increase over the next several seconds when the recovery period is prolonged. The recovery data for $I_{Ca(fc)}$ for the cell illustrated in Fig. 8*B* is well described by the sum of two exponentials with time constants of 203 ms and 4525 ms. In contrast, $I_{Ca(sc)}$ in the same cell recovers to its maximal value in less than 500 ms, and over a single exponential time course (Fig. 8*B*) with a time constant of 104 ms. At longer recovery times, however, $I_{Ca(sc)}$ amplitude *decreases* over a single exponential time course with a time constant of 8772 ms to a final, steady-state level (Fig. 8*B*). Similar results were obtained in many experiments ($n = 12$). Mean (±S.D.; $n = 12$) time constants for $I_{Ca(fc)}$ recovery at −90 mV were 357±73 ms and 3970±2519 ms, and mean (±S.D.; $n = 12$) time constants for $I_{Ca(sc)}$ recovery at −90 mV were 67±8 and 3846±1166 ms. The faster of the two time constants of recovery of $I_{Ca(fc)}$ and $I_{Ca(sc)}$ (i.e. 357±73 and 67±8 ms, respectively) are similar to the two time constants (875±543 and 77±6 ms) for recovery of $I_{Ca(peak)}$ to its maximal value (see above). These observations suggest that the two components of recovery of $I_{Ca(peak)}$ reflect the independent recoveries of $I_{Ca(fc)}$ and $I_{Ca(sc)}$. The similarity between the slower recovery time constants for $I_{Ca(fc)}$ and $I_{Ca(sc)}$, i.e. 3970±2519 and 3846±1166 ms, which correspond to the *increase* in $I_{Ca(fc)}$ and the *decrease* in $I_{Ca(sc)}$, respectively, suggests that the complete recovery of $I_{Ca(fc)}$ requires the prior recovery of $I_{Ca(sc)}$. That is, the slow phase of $I_{Ca(fc)}$ recovery appears to reflect the transition(s) from the $I_{Ca(sc)}$ to the $I_{Ca(fc)}$ pathway. Furthermore, both of these time constants are similar to the time constant for the slow decrease in $I_{Ca(peak)}$

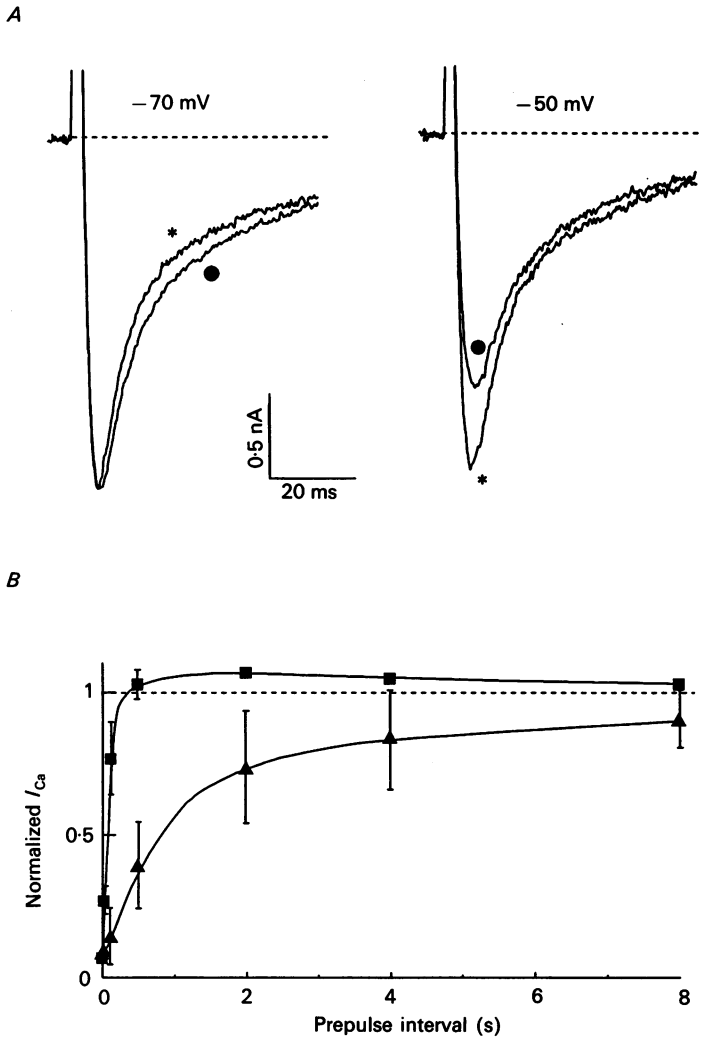

Fig. 9. Voltage dependence of the rate of recovery of I_{Ca} from steady-state inactivation. *A*, experiments were conducted as described in the legend of Fig. 8, except that the potential at which recovery was examined was changed to −70 mV (left panel) or −50 mV (right panel). The current waveforms displayed are those recorded when the recovery intervals at −70 and −50 mV were 1 s (*) and 8 s (●). Similar to the results obtained at −90 mV (Fig. 8), $I_{Ca(peak)}$ amplitude decreased and the decay rate was accelerated when the recovery period at −70 mV was increased from 1 to 8 s. At −50 mV, however, $I_{Ca(peak)}$ amplitude continues to increase when the recovery period increases from 1 to 8 s. *B*, mean (±S.D.) normalized recovery data for $I_{Ca(peak)}$ at −90 mV (■; $n = 12$) and −50 mV (▲; $n = 9$).

($\tau = 5053 \pm 2596$ ms), suggesting that the decrease in $I_{Ca(peak)}$ at long recovery times also reflects the transition from the $I_{Ca(sc)}$ to the $I_{Ca(fc)}$ pathway. In addition, these results suggest that transitions between the two gating pathways occur pre-

dominately, if not exclusively, via the closed states of the channel (see below and Discussion).

The possibility that the rate of recovery of I_{Ca} might be voltage dependent was explored in experiments identical to those described above, except that the holding potential and the interpulse voltages were varied to either −70 or −50 mV. The experiments at −70 mV revealed time-dependent changes in I_{Ca} similar to those observed at −90 mV (Fig. 8*A*). In particular, $I_{Ca(peak)}$ amplitudes decreased when the interpulse interval was increased from 1 to 8 s (Fig. 9*A*, left panel), and this decrease in peak current was accompanied by an acceleration of I_{Ca} decay. In addition, double exponential fits to the decay phases of the currents revealed an increase in $I_{Ca(fc)}$ and a decrease in $I_{Ca(sc)}$ on lengthening the interpulse interval from 1 to 8 s (data not shown). Similar results were obtained in many experiments and the mean (±S.D.; $n = 7$) normalized recovery data for $I_{Ca(peak)}$ recovery at −70 mV was well described by the sum of three exponentials with time constants of 276±32, 2336±107 and 5902±1426 ms (data not shown). Double exponential fits to the decay phases of the currents recorded at different recovery periods revealed that the faster two of these three time constants (i.e. 276±32 and 2336±107 ms) reflect the recoveries of $I_{Ca(sc)}$ and $I_{Ca(fc)}$, respectively. When these values are compared to those determined for recovery at −90 mV (above), it is clear that the recovery rates for $I_{Ca(fc)}$ and $I_{Ca(sc)}$ are markedly slowed at the more depolarized holding potential, whereas the rate of the transition(s) between the two pathways is only very slightly affected. When similar experiments were conducted at −50 mV, however, I_{Ca} recovery was markedly slowed and there was no *over-recovery* of $I_{Ca(peak)}$, as was evident at both −90 (Fig. 8) and −70 (Fig. 9*A*, left panel) mV. In fact, the amplitude of $I_{Ca(peak)}$ continued to increase when the recovery time at −50 mV was increased from 1 to 8 s (Fig. 9*A*, right panel). Similar results were obtained in nine cells, and mean (±S.D.) recovery data for $I_{Ca(peak)}$ at −50 mV are plotted in Fig. 9*B* as a function of interpulse interval. The mean normalized recovery data at −50 mV (Fig. 9*B*) are well described by the sum of two exponentials with time constants (±S.D.) of 893±101 and 9960±2191 ms. Double exponential fits to the decay phases of the currents recorded at different recovery periods revealed that these time constants reflect the recoveries of $I_{Ca(sc)}$ and $I_{Ca(fc)}$, respectively. Consistent with the recovery data at −70 mV, therefore, these results suggest the rates of recovery of both $I_{Ca(fc)}$ and $I_{Ca(sc)}$ are voltage dependent. Also, these analyses reveal that the transition from $I_{Ca(sc)}$ to $I_{Ca(fc)}$ is not readily resolved due primarily to the slow rate of recovery of $I_{Ca(fc)}$ at −50 mV.

Gating models of I_{Ca}

Taken together, all of the experimental results presented above are most simply interpreted as consistent with a model in which $I_{Ca(fc)}$ and $I_{Ca(sc)}$ reflect alternative pathways for gating of a single type of HVA Ca^{2+} channel. To test this hypothesis directly and to examine the molecular mechanisms underlying the gating of HVA Ca^{2+} channels in adult rat ventricular myocytes, a model involving two parallel gating pathways was developed (Fig. 10). The kinetic states C_{11}–C_{14}, O_1 and I_1 constitute the $I_{Ca(fc)}$ pathway and C_{21}–C_{24}, O_2 and I_2 constitute the $I_{Ca(sc)}$ pathway. The continuous lines between the various closed states in the two pathways reflect the fact that channels can distribute between the two pathways; the voltage-

dependent rate constants k_f and k_b govern these transitions. For simplicity, we assumed that the rate constants governing the transitions between each of the corresponding closed states were identical. The dashed lines between the two open states and those between the two inactivated states indicate that, based on the

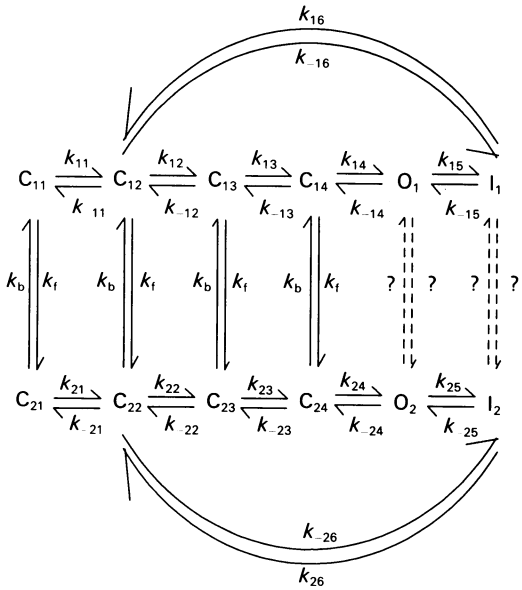

Fig. 10. Model of HVA Ca^{2+} channel gating in adult rat ventricular myocytes. Consistent with the experimental data, two parallel gating pathways are illustrated. As discussed in the text, the activation and deactivation rate constants in both pathways are assumed to be identical. The continuous lines between the various closed states indicate that interconversions between these states occur via the voltage-dependent forward and backward rate constants, k_f and k_b (see text). The dashed lines between the two open (O) and the two inactivated (I) states indicate uncertainty about whether these transitions are allowed (see text).

experimental data presented and discussed above, it is not possible to determine if these transitions occur (see below and Discussion). The model is illustrated with allowed transitions between the second, rather than the first, closed state and the inactivated state in each of the pathways because this was required to reproduce the experimental data. This finding suggests that inactivation is coupled to activation, rather than being independent, and is similar to recent models of voltage-dependent K^+ (Koren *et al.* 1990; Zagotta & Aldrich, 1990) and Na^+ (Vandenberg & Bezanilla, 1991) channel gating (see Discussion).

The experimental data reveal that the time constants of I_{Ca} activation do not vary measurably as a function of holding potential (Fig. 2*A*), and that current deactivation at all voltages is well described by a single exponential (Fig. 4). For the model, therefore, the activation rate constants in the fast pathway, k_{11} to k_{14}, and those in the slow pathway, k_{21} to k_{24}, were assumed to be the same. Similarly, the deactivation rate constants, k_{-11} to k_{-14} and k_{-21} to k_{-24}, for the two pathways were assumed to be identical. Because there is not a non-inactivating component of I_{Ca} in these cells (see above and Richard *et al.* 1990), there is no steady-state current

through the channels at depolarized potentials. As a result, inactivation was modelled with I_1 and I_2 being absorbing states, such that k_{-15} and k_{-25} equal zero at depolarized potentials. The rate constants for inactivation from the open states, k_{15} and k_{25}, were those derived from the analyses of the rates of I_{Ca} decay at each test

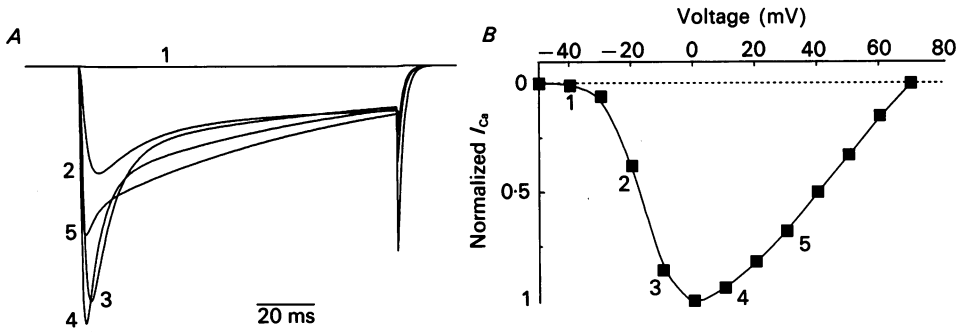

Fig. 11. The model reliably reproduces the waveforms (*A*) and the *I–V* relation (*B*) of I_{Ca} recorded in typical adult rat ventricular myocytes. *A*, using the model in Fig. 10 and the rate constants presented in the text, I_{Ca} waveforms were simulated. In this example, 90 and 10% of the channels were in the C_1 and C_2 pathways, respectively, at −90 mV at the onset of the depolarizations. In addition, the interpulse interval was long enough such that the channels reached steady-state at −90 mV between test depolarizations. *B*, peak *I–V* relation for the simulated currents displayed in *A*. The numbers identify the voltage steps at which the currents in *A* were simulated.

potential (Fig. 2*B*). Because neither τ_{fc} nor τ_{sc} varied substantially as a function of test potential (Fig. 2*B*), initial simulations were completed using average values for both inactivation rate constants. Also, in the initial simulations, the transitions from the inactivated to the closed states were assumed to be negligible at depolarized potentials and the rate constants governing these transitions, k_{-16} and k_{-26}, were set equal to 0. The rate constants for the C–I transitions were determined from the analyses of the kinetics of steady-state inactivation as a function of potential. The following expressions for k_{16} and k_{26} were derived: $k_{16} = 0{\cdot}4[\exp(-54\ V_m)]$ and $k_{26} = 0{\cdot}8[\exp(-26{\cdot}5\ V_m)]$. The voltage dependences of k_b and k_f were determined initially using the ratio C_1/C_2 at different holding potentials and defining this as k_b/k_f. The values of k_b and k_f were then adjusted until the model reliably reproduced the effects of changing the holding potential on I_{Ca} waveforms. The final forms of these rate constants were: $k_f = 70[\exp(70\ V_m)]$ and $k_b = 0{\cdot}1[\exp(40\ V_m)]$.

Using the model illustrated in Fig. 10 and the rate constants described above, simulated I_{Ca} waveforms evoked at various test potentials from a holding potential of −90 mV were generated. As shown in Fig. 11*A*, the waveforms of the simulated currents are remarkably similar to I_{Ca} waveforms measured in a typical adult rat ventricular myocyte (see, for example, Fig. 1). In addition, the model reliably reproduces the *I–V* relations for $I_{Ca(peak)}$ (Fig. 11*B*), as well as for $I_{Ca(fc)}$ and $I_{Ca(sc)}$ (data not shown). The model also allowed determination of the fraction of channels available for opening in the C_2 pathway, defined as $k_f/(k_f+k_b)$, as a function of holding potential. The model predicts that at a V_H of −90 mV, approximately 10% of the channels are in the C_2 pathway. The experimental data, however, suggest that,

on average, approximately 40% of the peak current is contributed by channels openings in the $I_{Ca(sc)}$ pathway on depolarization to +10 mV from a V_H of −90 mV (Fig. 3). The model reveals that this difference reflects the rapid rate of the transitions between the two pathways, i.e. k_f, at depolarized potentials; approxi-

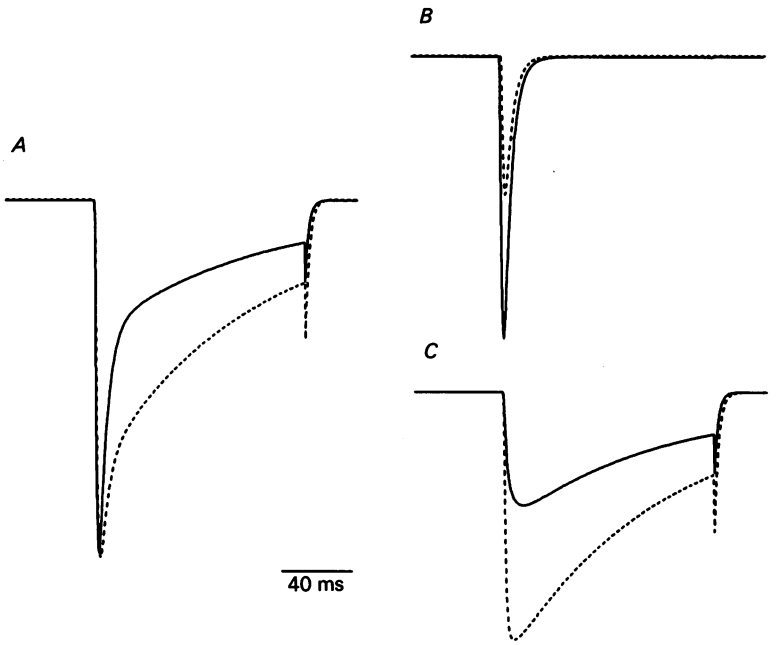

Fig. 12. Simulated I_{Ca} waveforms vary as a function of the V_H from which the currents are evoked. Current waveforms, simulated using the model illustrated in Fig. 10 and the rate constants given in the text, are displayed. The currents were modelled with steady-state distributions of 10 and 30% of the channels in the slow pathway and 90 and 70% of the channels in the fast pathway at steady state at −90 and −60 mV, respectively. *A*, simulated I_{Ca} waveforms for currents evoked at +10 mV from holding potentials of −90 (continuous line) and −60 (dashed line) mV: $I_{Ca(peak)}$ amplitude is increased and the apparent rate of I_{Ca} decay is slowed at the more depolarized V_H. Simulated $I_{Ca(fc)}$ (*B*) and $I_{Ca(sc)}$ (*C*) waveforms evoked on depolarizations to +10 mV from holding potentials of −90 (continuous lines) and −60 (dashed lines) mV. For currents evoked from −90 mV (continuous lines), $I_{Ca(fc)}$ amplitude is larger than $I_{Ca(sc)}$. When the V_H is changed to −60 mV (dashed lines), however, $I_{Ca(fc)}$ amplitude decreases, $I_{Ca(sc)}$ amplitude increases, and $I_{Ca(sc)}$ becomes the larger current component.

mately 30% of the channels in the C_1 pathway move to the C_2 pathway prior to opening. Based on the voltage dependence of k_f, the model also predicts that the ratio of $I_{Ca(fc)}/I_{Ca(sc)}$ will vary with test potential, as was observed experimentally (see Fig. 3*B*).

To test the validity of the model further, we examined the predicted effects on I_{Ca} waveforms of changing the holding potential and the frequency of current activation. As illustrated in Fig. 12*A*, the model reliably reproduces the effect of changing the holding potential on I_{Ca} waveforms. When the holding potential was changed from

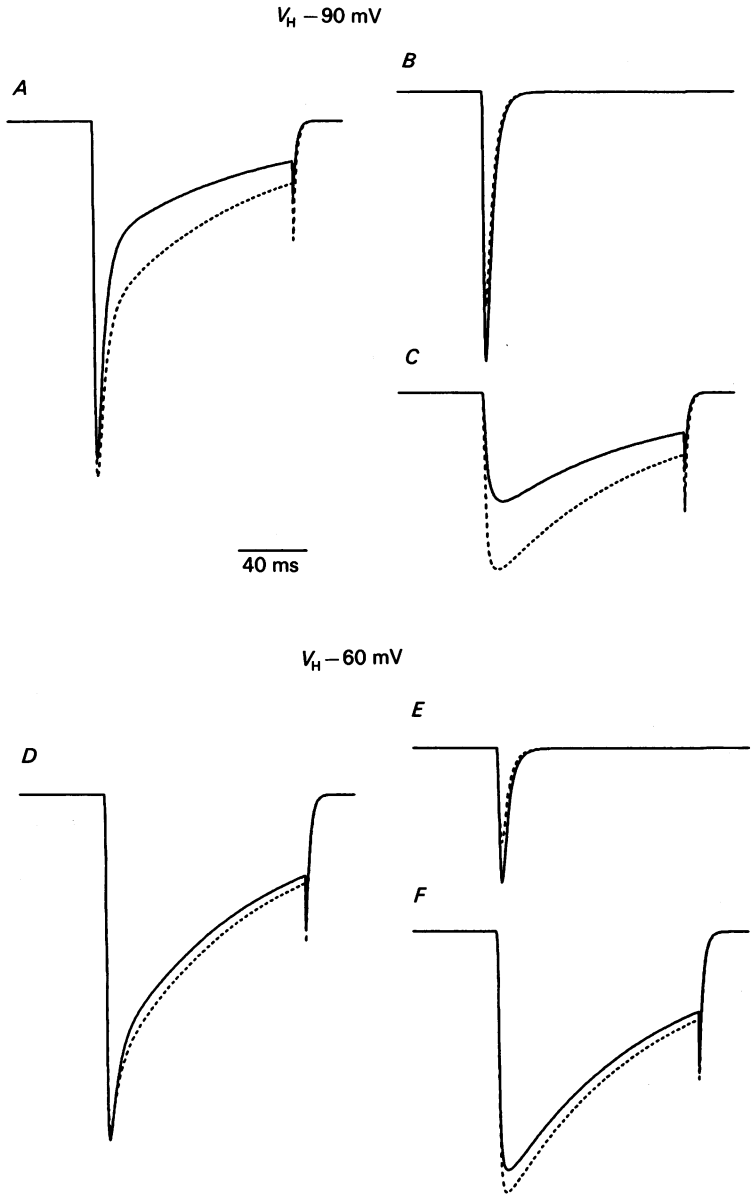

Fig. 13. Simulated I_{Ca} waveforms vary as a function of the frequency of current activation. Current waveforms evoked at +10 mV from holding potentials of −90 (*A–C*) and −60 (*D–F*) mV were simulated as described in the legend of Fig. 12, except that the time between the first (continuous lines) and the second (dashed lines) depolarizations was 500 ms. *A*, at 2 Hz, $I_{Ca(peak)}$ amplitude is increased and I_{Ca} decay is slowed in the second depolarization (dashed line). *B* and *C*, simulations of $I_{Ca(fc)}$ and $I_{Ca(sc)}$ waveforms revealed that the amplitude of $I_{Ca(fc)}$ (*B*) is decreased in the second depolarization, whereas the amplitude of $I_{Ca(sc)}$ (*C*) is increased. When the currents evoked from a V_H of −60 mV are simulated (*D*), the model predicts that increasing the frequency of activation results in a very slight slowing of I_{Ca} decay, and a slight *decrease* (rather than an increase) in $I_{Ca(peak)}$ amplitude. Simulations of $I_{Ca(fc)}$ (*E*) and $I_{Ca(sc)}$ (*F*) waveforms in this case revealed again

−90 to −60 mV, for example, there was a marked increase in $I_{Ca(peak)}$ amplitude evoked at +10 mV and a slowing of I_{Ca} decay (Fig. 12*A*), similar to what was observed experimentally (Fig. 5). The modelling revealed that this reflects the fact that changing the holding potential from −90 to −60 mV results in an increase in the fraction of channels in the C_2 pathway at steady state from about 10% at −90 mV to approximately 30% at −60 mV. Since approximately 30% of the channels that are in the C_1 pathway (at −60 mV before the depolarizing voltage step) also move into the C_2 pathway on depolarization and prior to opening, the net result is that approximately 50% of the channels open via the C_2 pathway on depolarization from the more depolarized holding potential. The net result, then, is that more channels open via the C_2 pathway when the V_H is −60 mV as compared to −90 mV, thereby resulting in an increase in $I_{Ca(peak)}$ and a slowing of I_{Ca} decay. In Fig. 12*B* and *C*, $I_{Ca(fc)}$ (*B*) and $I_{Ca(sc)}$ (*C*) waveforms simulated for depolarizations from −90 and −60 mV are displayed. As is evident, $I_{Ca(fc)}$ is larger for currents evoked from −90 mV (continuous lines in Fig. 12), whereas $I_{Ca(sc)}$ is larger for currents evoked from −60 mV (dashed lines in Fig. 12). Therefore, when the holding potential is depolarized from −90 to −60 mV, $I_{Ca(fc)}$ decreases and $I_{Ca(sc)}$ increases.

The model also reproduces the effects on I_{Ca} waveforms of changing the frequency of current activation. For currents evoked at +10 mV from a V_H of −90 mV, for example, the model predicts that increasing the frequency of activation from 0·2 to 2 Hz results in a large increase in $I_{Ca(peak)}$ amplitude and a slowing of I_{Ca} decay (Fig. 13*A*), similar to the frequency-dependent changes in I_{Ca} waveforms observed experimentally (Fig. 6). Three successive depolarizations were required to reach steady state. These simulations also revealed changes in the amplitudes of $I_{Ca(fc)}$ and $I_{Ca(sc)}$ (Fig. 13*B* and *C*) and the relative contributions of these two current components to $I_{Ca(peak)}$ as a function of activation frequency. When the frequency was increased from 0·2 to 2 Hz, for example, there was a substantial increase in $I_{Ca(sc)}$ amplitude (Fig. 13*C*) and a marked decrease in the amplitude of $I_{Ca(fc)}$ (Fig. 13*B*). Interestingly, the model predicts that when the holding potential is held more depolarized (e.g. at −60 mV), there is a slight decrease (rather than an increase) in $I_{Ca(peak)}$ amplitude, although the slowing of I_{Ca} is still evident (Fig. 13*D*). For currents evoked from −60 mV, $I_{Ca(sc)}$ (Fig. 13*F*) is much larger than $I_{Ca(fc)}$ (Fig. 13*E*), and there is only a slight increase in $I_{Ca(sc)}$ and a slight decrease in $I_{Ca(fc)}$ when the activation frequency was increased. Thus, the finding that I_{Ca} waveforms evoked from a V_H of −60 mV change only slightly with increased frequency of stimulation (Fig. 13*D*) appears to reflect the fact that a large fraction of the channels are already opening via the $I_{Ca(sc)}$ pathway at this holding potential.

As noted above, the modelling suggested that frequency-dependent changes in I_{Ca} waveforms will vary as a function of the holding potential from which the currents are evoked (Fig. 13). To test this prediction, I_{Ca} waveforms evoked at 1 Hz from various holding potentials were recorded. For currents evoked from −90 mV, $I_{Ca(peak)}$ amplitude is increased and current decay is slowed (Fig. 14); the changes in

---

that the amplitudes of $I_{Ca(fc)}$ and $I_{Ca(sc)}$ decrease and increase, respectively, with increasing frequency of activation. The increase in $I_{Ca(sc)}$ at this V_H, however, is small compared to that observed when the V_H is −90 mV (Fig. 13*C*).

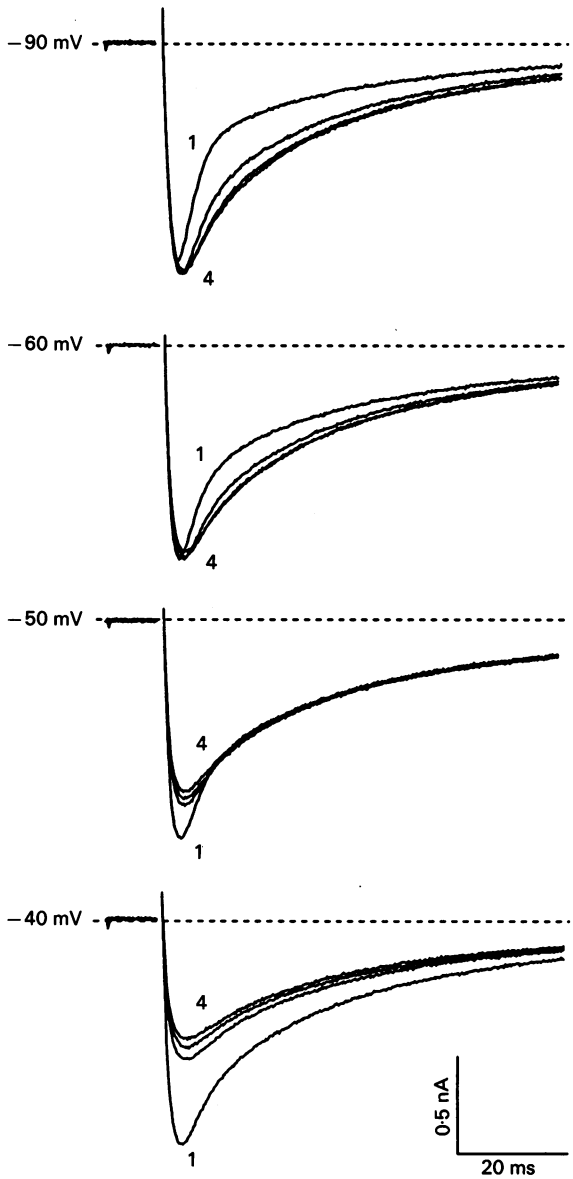

Fig. 14. Frequency-dependent changes in I_{Ca} waveforms vary as a function of the holding potential. Currents were evoked during depolarizations to +10 mV from various holding potentials as described in the legend of Fig. 1. In each panel, the currents recorded during four successive depolarizations presented at an interval of 1 s are displayed. From a V_H of −90 mV, $I_{Ca(peak)}$ amplitude increases and the rate of I_{Ca} decay is slowed on repetitive stimulation; steady state is reached in 2–3 s. For the currents evoked from −60 mV, $I_{Ca(peak)}$ amplitude increases slightly and there is a measurable increase in the time-to-peak I_{Ca} and a marked slowing of I_{Ca} decay; steady state is reached in 2–3 s. From more depolarized holding potentials, $I_{Ca(peak)}$ amplitudes decrease when the frequency of activation is increased. At a V_H of −40 mV, for example, $I_{Ca(peak)}$ amplitude is decreased approximately 40%, and 3–4 s are required to reach steady state (see text).

I_{Ca} waveforms reach steady state in 2–3 s. From more depolarized holding potentials (Fig. 14), however, quite different effects on I_{Ca} waveforms are observed. From a V_H of −60 mV, for example, $I_{Ca(peak)}$ amplitude was not measurably increased when the frequency of current activation was increased from 0·1 to 1 Hz, although the time-to-peak I_{Ca} increased slightly and I_{Ca} decay was markedly slowed (Fig. 14). Double exponential fits to the decay phases of the currents revealed that $I_{Ca(fc)}$ amplitude was decreased and $I_{Ca(sc)}$ amplitude was increased at the higher stimulation frequency. Therefore, although there was no significant change in $I_{Ca(peak)}$ amplitude when the interval between successive depolarizations from a V_H of −60 mV was decreased, there was a similar potentiation of $I_{Ca(sc)}$ and attenuation of $I_{Ca(fc)}$ to that observed for currents evoked from a V_H of −90 mV (see also Fig. 6). These observations are consistent with the predictions of the model (Fig. 13) discussed above. From a V_H of −50 mV, $I_{Ca(peak)}$ amplitude actually decreased on repetitive stimulation, although there was a measurable slowing of I_{Ca} decay (Fig. 14). A more marked decrease in $I_{Ca(peak)}$ on repetitive stimulation was seen when the holding potential was depolarized to −40 mV and current decay appeared monoexponential, suggesting the absence of the fast component, $I_{Ca(fc)}$ in this cell (Fig. 14). Similar results were obtained in several experiments and, on average, $I_{Ca(peak)}$ amplitudes evoked at +10 mV from a V_H of −40 mV decreased by 39±7% ($n = 6$) when the currents were recorded at 1 Hz (Fig. 14). Double exponential fits to the decay phases of the currents revealed that, for currents evoked from depolarized holding potentials, i.e. −50 and −40 mV, the amplitudes of both $I_{Ca(fc)}$ and $I_{Ca(sc)}$ were reduced, although $I_{Ca(fc)}$ was attenuated to a much larger extent. In agreement with the predictions of the modelling, therefore, these results are most simply interpreted as revealing that when the holding potential is depolarized from −90 to −60 to −40 mV, the slow rates of recovery from inactivation of both components predominate, and the peak current decreases as a result of cumulative inactivation.

DISCUSSION

Biphasic decay of I_{Ca}

The results presented here demonstrate the presence of two components of the macroscopic Ca^{2+} currents in isolated adult rat ventricular myocytes. These are referred to as $I_{Ca(fc)}$ and $I_{Ca(sc)}$ to denote the fast and slow components, respectively, of I_{Ca} decay. Although theoretically it is possible that the biexponential decay of I_{Ca} reflects contamination of the inward current waveforms by voltage-activated and/or Ca^{2+}-activated outward K^+ currents, we feel that this is unlikely for two reasons. First, depolarization-activated K^+ currents in these cells are effectively blocked by the Cs^+ in the recording pipettes and the TEA^+ in the bath (Richard *et al.* 1990; Apkon & Nerbonne, 1991). Second, we have found no experimental evidence to support the suggestion that there are Ca^{2+}-dependent K^+ currents in these cells (Apkon & Nerbonne, 1991). Taken together, these results suggest that the complex kinetic properties of I_{Ca} described here do not reflect contamination from unblocked voltage- or Ca^{2+}-activated outward K^+ currents.

Although initially distinguished on the basis of differing decay kinetics during depolarizing voltage steps, the *I–V* relations for $I_{Ca(fc)}$ and $I_{Ca(sc)}$ are distinct, and the

two current components display markedly different voltage and time dependences of steady-state inactivation. The rates of $I_{Ca(fc)}$ and $I_{Ca(sc)}$ activation and deactivation, however, are indistinguishable. As noted in the Introduction, the finding of two components of I_{Ca} decay could suggest the presence and activation of different types of voltage-gated Ca^{2+} channels (Bean, 1989; Hess, 1990) or, possibly, two distinct modes of gating of the same population of HVA Ca^{2+} channels (Hess *et al.* 1984; Pietrobon & Hess, 1990). Interestingly, alternative gating pathways of a single population of channels have been observed for both cloned Na^+ (Moorman *et al.* 1991; Zhou *et al.* 1991) and K^+ (Koren *et al.* 1990) channels expressed in *Xenopus* oocytes. Alternatively, two components of I_{Ca} decay could result from two distinct mechanisms of inactivation, such as Ca^{2+}-dependent and voltage-dependent inactivation mechanisms (Eckert & Chad, 1984), as has been demonstrated in other myocardial preparations (Kass & Sanguinetti, 1984; Lee *et al.* 1985).

Previously we argued that the properties of the two components of I_{Ca} in adult rat ventricular myocytes are not consistent with the suggestion that they reflect the presence and activation of two distinct populations of voltage-gated Ca^{2+} channels (Richard *et al.* 1990). Based on the measured time and voltage dependences of $I_{Ca(fc)}$ and $I_{Ca(sc)}$, for example, both components display properties consistent with their reflecting the currents through HVA-type Ca^{2+} channels (Bean, 1989; Hess, 1990). In addition, we have found no evidence to suggest that LVA Ca^{2+} channels (Bean, 1989; Hess, 1990) are also present in these cells (Richard *et al.* 1990). The properties of $I_{Ca(fc)}$ and $I_{Ca(sc)}$ are also not consistent with the suggestion that they simply reflect the dual presence of Ca^{2+}- and voltage-dependent inactivation mechanisms. Over the entire range of test voltages examined, for example, τ_{fc} and τ_{sc} vary by less than twofold, suggesting that neither component of I_{Ca} inactivation is markedly voltage dependent. In addition, and in contrast to what would be expected for a voltage-dependent component of I_{Ca} inactivation (Fox, 1981; Kass & Sanguinetti, 1984; Jones & Marks, 1989), the trend for both time constants is to *increase* with increasing depolarization rather than to *decrease*. The finding that neither τ_{fc} nor τ_{sc} varies appreciably as a function of I_{Ca} amplitude might be interpreted as revealing that current inactivation is not measurably Ca^{2+} or current dependent. Nevertheless, both time constants are approximately an order of magnitude faster than those measured when either Ba^{2+} or Sr^{2+} is used in place of Ca^{2+} as the charge carrier (Richard *et al.* 1990), suggesting that the rates of inactivation of *both* current components are Ca^{2+} sensitive (see also below).

Of the three possible mechanisms proposed to account for the two components of I_{Ca} inactivation, therefore, the time- and voltage-dependent properties of the currents are most simply interpreted in terms of a model in which $I_{Ca(fc)}$ and $I_{Ca(sc)}$ reflect alternate pathways for the gating of a single population of HVA Ca^{2+} channels. Furthermore, the observed voltage-, time- and frequency-dependent changes in $I_{Ca(fc)}$ and $I_{Ca(sc)}$ amplitudes are also consistent with a dual gating pathway model in which the two current components are not independent and in which interconversions between the two pathways occur. Nevertheless, it is important to note that similar time- and/or voltage-dependent potentiation of cardiac HVA Ca^{2+} channel currents has been described by others (Lee, 1987; Argibay *et al.* 1988; Fedida, Noble & Spindler, 1988*a*, *b*; Tseng, 1988; Schouten & Morad,

1989; Zygmunt & Maylie, 1990; Pietrobon & Hess, 1990) at both the macroscopic and the single channel current levels. The molecular interpretations of these observations have varied widely among different authors, however, and all of the proposed models differ in important ways from the dual, interconverting gating pathway model proposed here (see also below).

Two parallel pathways for Ca^{2+} channel gating

To test the validity of our interpretation of the experimental data that $I_{Ca(fc)}$ and $I_{Ca(sc)}$ reflect two parallel pathways for gating a single population of HVA Ca^{2+} channels, a gating model was developed (Fig. 10). The important features of the model, based on the experimental data and required to simulate the macroscopic I_{Ca} waveforms are: (1) four closed states prior to channel opening; (2) inactivation from both the open and closed states; and, (3) two parallel pathways for gating linked via the closed states. Although closed state inactivation was required, the simulations also revealed that transitions from the second closed state to the inactivated state in each pathway reliably reproduced the experimental data, whereas transitions from the first closed states to the inactivated states did not. These findings suggest that inactivation is not independent, but rather is coupled to channel activation. A similar conclusion has been reached in recent analyses of K^+ (Koren *et al.* 1990; Zagotta & Aldrich, 1990) and Na^+ (Vandenberg & Bezanilla, 1991) channels, suggesting some commonality in the gating mechanisms of many different types of voltage-dependent ion channels.

In addition to generating I_{Ca} waveforms and I–V relations similar to those recorded in the typical adult rat ventricular myocyte, the model also reproduced the experimentally observed voltage- and frequency-dependent changes in I_{Ca} waveforms. Constructing the model and examining the waveforms of the simulated currents under various conditions also allowed us to explore the likely kinetic states linking the two pathways. In this context, the model revealed that the increase in $I_{Ca(peak)}$ amplitude and the slowing of I_{Ca} decay observed experimentally when the holding potential was changed from -90 to -50 mV could be accounted for by including voltage-dependent transitions between closed channels in the two pathways. Previously, we suggested that the observation that the amplitudes of $I_{Ca(sc)}$ evoked from hyperpolarized holding potentials increase at high stimulation frequencies could reflect transitions between the inactivated states of the channel in the slow and the fast pathways (Richard *et al.* 1990). The simulations revealed, however, that the simplest model to account for the experimental data is one in which transitions between the two pathways occur *only* via the closed states of the channel. In fact, in the model, the voltage dependence of the transitions between the closed states of the channel in the two pathways accounts completely for the frequency-dependent potentiation of the currents and for the *over-recovery* of $I_{Ca(peak)}$ and $I_{Ca(sc)}$ amplitudes observed during the recovery of the currents from steady-state inactivation at hyperpolarized potentials. Clearly, the finding that all of the experimental data can be accounted for when the model includes transitions *only* between the closed states does not mean that transitions between the open and/or inactivated states does not occur; it simply means that these transitions are not necessary to account for the macroscopic properties of the currents.

As noted above, several laboratories have reported time- and/or voltage-dependent facilitation of cardiac HVA Ca^{2+} channel currents (Lee, 1987; Argibay *et al.* 1988; Fedida *et al.* 1988*a*, *b*; Tseng, 1988; Schouten & Morad, 1989; Zygmunt & Maylie, 1990; Pietrobon & Hess, 1990), although the interpretations of the molecular mechanisms underlying the observed effects have varied considerably. Lee (1987), for example, described frequency-dependent potentiation of I_{Ca} amplitudes and slowing of I_{Ca} decay in guinea-pig ventricular myocytes. In contrast to the model proposed here, however, those results were interpreted as reflecting the population of a long-lived open state (populated from the first open state in a sequential gating pathway) that was not normally populated at low rates of channel activation (Lee, 1987). Also, in contrast to the findings here, potentiation of the currents during repetitive stimulation was seen when Ba^{2+} was used (in place of Ca^{2+}) as the charge carrier, and it has been suggested by some investigators that facilitation of the HVA Ca^{2+} channel currents in guinea-pig (Lee, 1987) and frog (Schouten & Morad, 1989) ventricular myocytes is voltage dependent. A similar voltage-dependent mechanism has been proposed to explain the observation that, on strong depolarizations, single L-type (HVA) cardiac Ca^{2+} channels can switch to a different gating model (Hess *et al.* 1984) that is characterized by long openings and high open probability (Pietrobon & Hess, 1990). In contrast to the results here, however, the observed transitions between different gating modes are much slower than the transitions between different kinetic states within the same mode (Hess *et al.* 1984; Pietrobon & Hess, 1990). Similar to previous studies on frog (Argibay *et al.* 1988), guinea-pig (Fedida *et al.* 1988*a*, *b*; Zygmunt & Maylie, 1990) and canine (Tseng, 1988) ventricular myocytes, however, we find that the frequency-dependent potentiation of HVA Ca^{2+} channel currents in adult rat ventricular myocytes is *only* evident when Ca^{2+} is used as the charge carrier. These results are most simply interpreted as suggesting that, in addition to being voltage dependent, the gating mechanism itself and the switch between the two gating pathways in adult rat ventricular myocytes are also Ca^{2+} dependent or Ca^{2+} sensitive (see also below).

Previously it was reported that increasing the frequency of current activation results in a decrease in I_{Ca} amplitudes in adult rat ventricular myocytes (Mitchell, Powell, Terrar & Twist, 1985). This finding was interpreted as reflecting an increase in Ca^{2+}-dependent inactivation of I_{Ca} due to the Ca^{2+}-dependent release of intracellular Ca^{2+} (Mitchell *et al.* 1985). These findings were in apparent conflict with our observations that increasing the frequency of I_{Ca} activation results in an increase in $I_{Ca(peak)}$ amplitude and a slowing of I_{Ca} decay (Fig. 6; see also Richard *et al.* 1990). When modelling the currents, however, we found that the model predicted that frequency-dependent changes in I_{Ca} waveforms would be expected to vary with the membrane potential from which the currents are evoked and, in subsequent experiments, this prediction was shown to be correct. For currents evoked from holding potentials between -90 and -60 mV, for example, peak I_{Ca} amplitudes increased when the frequency of I_{Ca} activation was increased. For currents evoked from more depolarizing holding potentials, in contrast, increasing the frequency of stimulation decreased I_{Ca}. These observations can be accounted for completely in the model here by the voltage dependences of the transitions between the closed states linking the two gating pathways and the voltage dependences of the rates of recovery

from inactivation of both $I_{Ca(fc)}$ and $I_{Ca(sc)}$. A similar dependence on the holding potential has been reported for the frequency-dependent potentiation of I_{Ca} in frog ventricular myocytes (Schouten & Morad, 1989), suggesting the interesting possibility that a dual gating pathway may also be operative in these cells.

Ca^{2+} dependence of HVA Ca^{2+} channel gating

When Ca^{2+} is replaced by either Ba^{2+} or Sr^{2+}, current decay also follows a biexponential time course, although both decay time constants are approximately an order of magnitude larger than τ_{fc} and τ_{sc} for I_{Ca} decay (Richard *et al.* 1990). In addition, we find that neither the voltage- nor the frequency-dependent potentiation of the Ca^{2+} channel currents is observed when Ba^{2+} or Sr^{2+} is used in place of Ca^{2+} as the charge carrier. Taken together, these findings clearly suggest that Ca^{2+} plays an important role in determining the kinetics of HVA Ca^{2+} channel gating in adult rat ventricular myocytes. Unexpectedly, however, we found that changing the type or the concentration of the Ca^{2+} buffer in the recording pipettes did not markedly influence the measured current waveforms (data not shown). Lowering the EGTA concentration in the recording pipettes to 1 mM ($n = 14$) or using 10 mM BAPTA (Tsien, 1980) ($n = 7$) in place of EGTA, for example, did not measurably affect the properties of the currents. Indeed, I_{Ca} waveforms recorded under both of these conditions were indistinguishable from those recorded in the presence of 10 mM EGTA ($n = 17$), and there were no measurable changes in τ_{fc} and τ_{sc} or in the voltage dependences of $I_{Ca(fc)}$ and $I_{Ca(sc)}$. In addition, the voltage- and frequency-dependent changes in I_{Ca} amplitudes and kinetics were similar when recordings were obtained with 10 mM BAPTA-containing pipettes ($n = 7$). Nevertheless, it is clear that the kinetic properties of the currents, as well as the voltage- and frequency-dependent changes in the current waveforms, are seen *only* when Ca^{2+} is present in the extracellular solution and carrying the current through the channels. Thus, in spite of the apparent insensitivity to changes in the concentration or the type of intracellular Ca^{2+} buffer, we must conclude that the measured properties of the currents are Ca^{2+} dependent or, perhaps more appropriately, are Ca^{2+} sensitive.

The mechanisms underlying this apparent Ca^{2+} dependence (sensitivity) of the rates of I_{Ca} inactivation and of the frequency- and voltage-dependent potentiation of I_{Ca} in adult rat ventricular myocytes are unclear. The similarity between the effects of high-frequency stimulation and β-adrenergic receptor activation led Fedida and co-workers (1988*a*, *b*) to suggest that facilitation of I_{Ca} in guinea-pig ventricular myocytes reflects a change in Ca^{2+} channel phosphorylation. Zygmunt & Maylie (1990), however, suggested that it was more likely that Ca^{2+} affected some step in the cascade linking β-receptor activation to Ca^{2+} channel modulation, rather than phosphorylating the Ca^{2+} channels directly. Direct changes in intracellular Ca^{2+}, produced by light flashes in the presence of the photolabile Ca^{2+} chelator nitr-5, have been shown to increase I_{Ca} amplitudes in frog and guinea-pig myocytes (Gurney, Charnet, Pye & Nargeot, 1989; Charnet *et al.* 1991). In addition, the kinetics of the increases in I_{Ca} amplitude seen in response to intracellular Ca^{2+} concentration jumps were similar to those seen in response to β-receptor activation (Gurney *et al.* 1989; Charnet *et al.* 1991), consistent with the view that Ca^{2+} may modulate Ca^{2+} channel activity through a phosphorylation-dependent mechanism. The frequency-depen-

dent potentiation of I_{Ca} in adult rat ventricular myocytes described here, however, is fast – probably too fast to be accounted for by a mechanism involving phosphorylation either of the Ca^{2+} channel itself or of some closely associated regulatory molecule, although we cannot rule out this possibility with the data presently available. An alternative interpretation of our results is that Ca^{2+} ions influence the gating of the Ca^{2+} channels directly. If correct, then the lack of effect of lowering the EGTA concentration or of using BAPTA in the recording pipettes further suggests that the site at which Ca^{2+} is affecting channel gating must be within or very close to the channel pore. In support of this view, recent single channel studies have revealed that Ca^{2+} entry during the opening of a single Ca^{2+} channel produces rapid changes in the gating transition rates (Yue, Backx & Imredy, 1990). Further studies aimed at determining the site(s) of action of Ca^{2+} and the detailed mechanism(s) involved in mediating the apparent Ca^{2+} dependence of I_{Ca} inactivation and the time- and voltage-dependent facilitation of I_{Ca} in adult rat ventricular myocytes are clearly warranted.

We thank Drs Michael Apkon, Joel Nargeot and François Tiaho for many helpful comments and discussions throughout the course of this work. We also acknowledge the financial support provided by the French Ministère des Relations Extérieures (Bourse Lavoisier), the Fondation de France (postdoctoral fellowship to S.R.), the North Atlantic Treaty Organization (International Collaborative Research Grant No. 900545 to S.R.), the American Heart Association (Established Investigator Award and Grant-in-Aid to J.M.N.), and the National Institutes of Health (No. HL34161 to J.M.N.)

REFERENCES

APKON, M. & NERBONNE, J. M. (1991). Characterization of two distinct depolarization-activated K^+ currents in isolated adult rat ventricular myocytes. *Journal of General Physiology* **97**, 973–1011.

ARGIBAY, J. A., FISCHMEISTER, R. & HARTZELL, H. C. (1988). Inactivation, reactivation and pacing dependence of calcium current in frog cardiocytes: correlation with current density. *Journal of Physiology* **401**, 201–226.

BEAN, B. P. (1985). Two kinds of calcium channels in canine atrial cells. *Journal of General Physiology* **86**, 1–30.

BEAN, B. P. (1989). Classes of calcium channels in vertebrate cells. *Annual Review of Physiology* **51**, 367–384.

BONVALLET, R. & ROUGIER, O. (1989). Existence of two calcium currents recorded at normal calcium concentrations in single frog atrial cells. *Cell Calcium* **10**, 499–508.

ECKERT, R. & CHAD, J. E. (1984). Inactivation of Ca channels. *Progress in Biophysics and Molecular Biology* **44**, 215–267.

EHARA, T., NOMA, A. & ONO, K. (1988). Calcium-activated non-selective cation channels in ventricular cells isolated from adult guinea-pig hearts. *Journal of Physiology* **403**, 117–133.

FEDIDA, D., NOBLE, D. & SPINDLER, A. J. (1988*a*). Use-dependent reduction and facilitation of Ca^{2+} currents in guinea-pig myocytes. *Journal of Physiology* **405**, 439–460.

FEDIDA, D., NOBLE, D. & SPINDLER, A. J. (1989*b*). Mechanism of the use dependence of Ca^{2+} current in guinea-pig myocytes. *Journal of Physiology* **405**, 461–475.

FOX, A. P. (1981). Voltage-dependent inactivation of a calcium channel. *Proceedings of the National Academy of Sciences of the USA* **78**, 953–956.

GURNEY, A. M., CHARNET, P., PYE, J. M. & NARGEOT, J. (1989). Augmentation of cardiac calcium current by flash photolysis of intracellular caged Ca^{2+} molecules. *Nature* **341**, 65–68.

HAGIWARA, N., IRISAWA, H. & KAMEYAMA, M. (1988). Contribution of two types of calcium currents to the pacemaker potentials of rabbit sino-atrial node cells. *Journal of Physiology* **395**, 233–253.

HAGIWARA, S., OZAWA, S. & SAND, O. (1975). Voltage-clamp analysis of two inward current mechanisms in the egg cell membrane of a starfish. *Journal of General Physiology* **65**, 617–644.

HAMILL, O. P., MARTY, A., NEHER, E., SAKMANN, B. & SIGWORTH, F. J. (1981). Improved patch-clamp techniques for high-resolution current recording from cells and cell-free membrane patches. *Pflügers Archiv* **391**, 85–100.

HESS, P. (1990). Calcium channels in vertebrate cells. *Annual Review of Neuroscience* **13**, 337–356.

HESS, P., LANSMAN, J. B. & TSIEN, R. W. (1984). Different modes of Ca channel gating behaviour favoured by dihydropyridine Ca agonists and antagonists. *Nature* **311**, 538–544.

JONES, S. W. & MARKS, T. N. (1989). Calcium currents in bullfrog sympathetic neurons. II. Inactivation. *Journal of General Physiology* **94**, 169–182.

KASS, R. S. & SANGUINETTI, M. C. (1984). Calcium channel inactivation in the calf cardiac Purkinje fiber: evidence for voltage- and calcium-mediated mechanisms. *Journal of General Physiology* **84**, 705–726.

KOREN, G., LIMAN, E. R., LOGOTHETIS, D. E., NADAL-GINARD, B. & HESS, P. (1990). Gating mechanism of a cloned potassium channel expressed in frog oocytes and mammalian cells. *Neuron* **2**, 39–51.

LEE, K. S. (1987). Potentiation of the calcium-channel currents of internally perfused mammalian heart cells by repetitive depolarizations. *Proceedings of the National Academy of Sciences of the USA* **84**, 3941–3945.

LEE, K. S., MARBAN, E. & TSIEN, R. W. (1985). Inactivation of calcium channels in mammalian heart cells: joint dependence on membrane potential and intracellular calcium. *Journal of Physiology* **364**, 395–411.

LEGRAND, B., HATEM, S., DEROUBAIX, E., COUETIL, J. P. & CORABOEUF, E. (1991). Calcium current depression in isolated human atrial myocytes after cessation of chronic treatment with calcium antagonists. *Circulation Research* **69**, 292–300.

MARTY, A. & NEHER, E. (1983). Tight-seal whole-cell recording. In *Single Channel Recording*, ed. SAKMANN, B. & NEHER, E., pp. 107–122. Plenum Press, New York.

MITCHELL, M. R., POWELL, T., TERRAR, D. A. & TWIST, V. W. (1985). Influence of a change in stimulation rate on action potentials, currents and contractions in rat ventricular cells. *Journal of Physiology* **364**, 113–130.

MITRA, R. & MORAD, M. (1986). Two types of calcium channels in guinea-pig ventricular myoctes. *Proceedings of the National Academy of Sciences of the USA* **83**, 5340–5344.

MOORMAN, J. R., KIRSCH, G. E., VANDONGEN, A. M., JOHO, R. H. & BROWN, A. M. (1990). Fast and slow gating of sodium channels encoded by a single mRNA. *Neuron* **4**, 243–252.

NILIUS, B., HESS, P., LANSMAN, J. B. & TSIEN, R. W. (1985). A novel type of cardiac calcium channel in ventricular cells. *Nature* **316**, 443–446.

OUADID, H., SEGUIN, J., RICHARD, S., CHAPTAL, P. A. & NARGEOT, J. (1991). Properties and modulation of Ca channels in adult human atrial cells. *Journal of Molecular and Cellular Cardiology* **23**, 41–54.

PIETROBON, D. & HESS, P. (1990). Novel mechanism of voltage-dependent gating in L-type calcium channels. *Nature* **346**, 651–655.

RICHARD, S., TIAHO, F., CHARNET, P., NARGEOT, J. & NERBONNE, J. M. (1990). Two pathways for Ca^{2+} channel gating differentially modulated by physiological stimuli. *American Journal of Physiology* **258**, H1872–1881.

SCHOUTEN, V. J. A. & MORAD, M. (1989). Regulation of Ca^{2+} current in frog ventricular myocytes by holding potential, c-AMP and frequency. *Pflügers Archiv* **415**, 1–11.

TSENG, G.-N. (1988). Calcium current restitution in mammalian ventricular myocytes is modulated by intracellular calcium. *Circulation Research* **63**, 468–482.

TSIEN, R. Y. (1980). New calcium indicators and buffers with high selectivity against magnesium and protons: design, synthesis, and properties of prototype structures. *Biochemistry* **19**, 2396–2404.

VANDENBERG, C. A. & BEZANILLA, F. (1991). A sodium channel gating model based on single channel, macroscopic ionic, and gating currents in the squid giant axon. *Biophysical Journal* **60**, 1511–1533.

XU, X. & BEST, P. M. (1990). Increase in T-type calcium current in atrial myocytes from adult rats with growth hormone-secreting tumors. *Proceedings of the National Academy of Sciences of the USA* **12**, 4655–4659.

YUE, D. T., BACKX, P. H. & IMREDY, J. P. (1990). Calcium-sensitive inactivation in the gating of single calcium channels. *Science* **250**, 1735–1738.

YUE, D. T., HERZIG, S. & MARBAN, E. (1990). Beta-adrenergic stimulation of calcium channels occurs by potentiation of high-activity gating modes. *Proceedings of the National Academy of Sciences of the USA* **87**, 753–757.

ZAGOTTA, W. N. & ALDRICH, R. W. (1990). Voltage-dependent gating of *Shaker* A-type potassium channels in *Drosophila* muscle. *Journal of General Physiology* **95**, 29–60.

ZHOU, J., POTTS, J. F., TRIMMER, J. S., AGNEW, W. S. & SIGWORTH, F. J. (1991). Multiple gating modes and the effects of modulating factors on the μI sodium channel. *Neuron* **7**, 775–785.

ZYGMUNT, A. C. & MAYLIE, J. (1990). Stimulation-dependent facilitation of the high threshold calcium current in guinea-pig ventricular myocytes. *Journal of Physiology* **428**, 653–671.